Inferring the initiation and development of Myeloproliferative Neoplasms

Gurvan Hermange[1], Alicia Rakotonirainy[1], Mahmoud Bentriou[1], Amandine Tisserand[2, 3, 4], Mira El-Khoury[2, 3, 4], François Girodon[6,7], Christophe Marzac[8], William Vainchenker[2, 3, 5], Isabelle Plo[2, 3, 5], and Paul-Henry Cournède[1]

[1]Université Paris-Saclay, CentraleSupélec, Laboratory of Mathematics and Informatics (MICS), Gif-sur-Yvette, France.
[2]INSERM U1287 (INSERM, Gustave Roussy, Université Paris-Saclay), Villejuif, France
[3]Gustave Roussy, Villejuif, France
[4]Université de Paris (Paris Diderot), Paris, France
[5]Université Paris-Saclay, Villejuif, France
[6]Laboratoire d'Hématologie, CHU Dijon, Dijon, France
[7]INSERM, UMR866, Centre de Recherche, Dijon, France
[8]Laboratoire d'Immuno-Hématologie, Gustave Roussy, Villejuif

Supplemental Material

We base our method on a mathematical model, presented in more details in section A. First, in § A.1, we describe the stochastic model of the clonal expansion from a single mutated hematopoietic stem cell (HSC), in § A.2 we describe how we model the progenitor and mature cell compartments, then we explain how we model the acquisition of the driver mutation in § A.3 and eventually which values or prior distributions we consider for the parameters (§ A.4).
Inferring the initiation and development of Myeloproliferative Neoplasms (MPNs) relies on the estimation of model parameters using observations. We detail the parameter estimation procedure in section B, where we introduce the ABC-SMC method (§ B.1). We also detail how we derive a deterministic approximation of our stochastic model after some time in (§B.2). To optimize the estimation process, we use the Hungarian algorithm, it is described in (§ B.3). We end this section by giving some information on the model implementation (§ B.4).
We further show that we can draw robust conclusions from our parameter estimation procedure in section C, by inferring parameter values from synthetic data (§ C.1) We explore potential biases in the estimation of parameters λ (§ C.2) and Δ (§ C.3).
Then, in section D, we conduct the analysis based on real data (§ D.1), detail our results (§ D.2) and conduct a leave-one-out analysis (§ D.3) to further assess the quality of the model fits.
We finally compare, in section E, our results to other reports, concerning the mean acquisition time (§ E.1) or the proliferative advantage (§ E.2) of the mutation $JAK2^{V617F}$.

A Model

A.1 Stochastic description of the disease development

The model we propose (main figures 1.B and 1.D) aims to describe the expansion of a malignant clone from a single mutated HSC. We assume that the number of wild-type (WT) cells N_{WT} is maintained constant through a tight regulatory mechanism, corresponding to homeostatic conditions. T_0 is the age at which the first mutation to the considered gene (either *CALR* or *JAK2*) is acquired. We will study the dynamics of $N(t)$, the number of mutated HSCs, over time $t \geq T_0$ (with $N(T_0) = 1$).
Mutated HSCs divide at a rate α. Three division mechanisms are widely accepted for HSCs. First, an HSC can encounter a differentiated division (diff), with a probability p_0, and generate two (very immature) progenitor cells. Progenitor cells will further proliferate and differentiate, resulting in the production of our blood cells (see § A.2). Secondly, an HSC can divide asymmetrically (asym), with a probability p_1, giving a progenitor cell and a stem cell, this latter being functionally identical to the

mother cell. And finally, an HSC can divide symmetrically (sym), with a probability $p_2 = 1 - p_1 - p_0$, producing two HSCs (see eq. (1)).
In this article, we focus on HSCs, since they are at the origin of hematopoiesis (that is, the production of all types of blood cells). We introduce $\Delta = p_2 - p_0$. For WT cells, this parameter is equal to zero in order to maintain homeostatic conditions. We consider that cells with mutations have a proliferate advantage at the stem cell level, i.e. $\Delta > 0$ (otherwise the probability of extinction would be equal to 1).
If the time between divisions was constant, the process described above would be a standard multi-type branching process, widely used to model cell proliferation processes [4]. In that case, we could compute a probability of extinction for the mutated stem cells equal to $q = p_0/p_2 < 1$ (since we assume that $\Delta > 0$).
In our model, the time between two divisions is not constant but follows an exponential distribution with rate equal to α. Thus, the number $N(t)$ of mutated cells and its potential expansion over time t follows a stochastic process that can be described as a Continuous Time Markov Chain (CTMC). It can also be written using the formalism of chemical reaction networks:

$$\begin{array}{ll} \text{diff}: & \text{HSC} \xrightarrow{\alpha p_0} \emptyset \\ \text{asym}: & \text{HSC} \xrightarrow{\alpha p_1} \text{HSC} \\ \text{sym}: & \text{HSC} \xrightarrow{\alpha p_2} 2\text{HSC} \end{array} \tag{1}$$

With this process, there is a probability $q = p_0/p_2$ that the mutated clone naturally extincts. If it does not disappear, the mutated clone will expand over time, until the number of mutated HSCs becomes potentially very high. This type of model describing the expansion of a malignant clone is classical, and not far from the one used for example by Watson et al. [12].
Throughout all the article, we focus on trajectories without extinction.

A.2 Description of the last hematopoietic stages

The stochastic process introduced in the previous paragraph describes the dynamics of mutated HSCs. Yet, in practice, it is not possible to obtain information for true HSCs, but rather progenitor cells (or mature cells in clinical routine). Then, to confront our model with experimental observations (see § D.1), we also have to describe the dynamics of the last stages of hematopoiesis. In our model, we then introduce two additional compartments: one for progenitor cells and one for mature cells (see Fig. A.1). At the level of stem cells, we consider the dynamics $N(t)$ of the number of mutated HSCs over time $t > T_0$. But observations associated with progenitor cells or mature cells are not direct measures of the number of mutated cells but rather proportions.

Considering that, on average, over a short time δt, $\alpha\delta t N_{WT}$ wild-type HSCs generate the same quantity of progenitor cells (since there is a balance between differentiated and symmetrical divisions to ensure homeostatic conditions of these healthy cells) and $\alpha\delta t N$ mutated HSCs will give birth to $\alpha(1-\Delta)\delta t N$ immature progenitor cells, we get for the clonal fraction (CF) of progenitor cells:

$$\eta(t) = \frac{(1-\Delta)N(t)}{(1-\Delta)N(t) + N_{WT}} \tag{2}$$

Actually, relation (2) is an approximation that would not be totally correct in the early stages of the disease expansion, when the number of mutated HSCs is too low. When the patients are diagnosed, however, the malignant clone has already expanded, and our relation becomes valid.

Progenitor cells then give rise to mature cells. In clinical routine, instead of measuring a CF, that is, a proportion of mutated cells, we measure a variant allele frequency (VAF), that is, a proportion of mutated alleles. In this study, since we only consider heterozygous mutated cells, the CF is twice the percentage of the VAF. To note that the term CF is generally associated with progenitor cells when the term VAF will always refers - in our study - to a VAF measure in peripheral blood. The VAF measure is not a good proxy for the CF among progenitors since $JAK2^{V617F}$ but also, to a lesser extent, $CALR^m$ progenitor and precursor cells proliferate more than WT cells during the latest stages

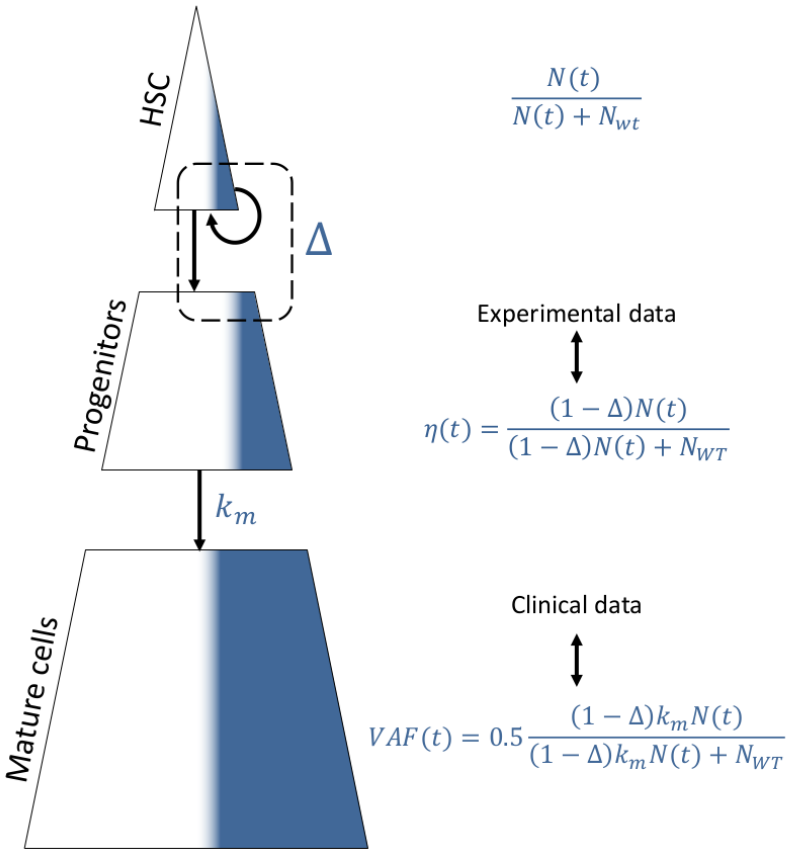

Figure A.1: Schematic representation of our model. At the apex of the hematopoietic tree, we find the HSCs that can self-renew. If $N(t)$ represents the number of mutated HSCs and N_{WT} the number of WT HSCs, the CF among this compartment at time t would be equal to $\frac{N(t)}{N(t)+N_{WT}}$. Yet, HSCs can not be observed. What can be measured is the CF among progenitor cells $\eta(t)$. Our model parameters, notably Δ, representing the balance between symmetric and differentiated divisions for mutated HSCs, can be inferred based on the measure of CF among progenitor cells. Then, progenitor cells expand and differentiate to become mature cells that ultimately die. Mutated progenitor cells would also have a proliferative advantage over WT cells, so one mutated progenitor cell will lead to more mature cells compared to a WT progenitor cell. This proliferative advantage at the level of committed cells is described by parameter k_m. In clinical routine, the VAF among mature cells is measured.

of hematopoiesis. Extending eq. (2), the VAF in peripheral blood at time t is equal to:

$$VAF(t) = 0.5\frac{(1-\Delta)k_m N(t)}{(1-\Delta)k_m N(t)+N_{WT}} \tag{3}$$

where k_m models the proliferative advantage of mutated cells, from progenitors to mature cells, compared to WT cells. This parameter was introduced and estimated by Mosca et al. [8], and its value was estimated at around 7.5 for $JAK2^{V617F}$ cells and 5.0 for $CALR^m$.

A.3 Acquisition of the mutation

The stochastic process presented above starts with one mutated cell at time $t = T_0$. The process and dynamics of the acquisition of driver mutations are still a matter of debate, with different studies leading to different conclusions in the case of the mutation $JAK2^{V617F}$ and no study exists at all for the mutation to the gene *CALR*. Williams et al. [14] reported cases in which the mutation $JAK2^{V617F}$ was acquired during fetal life. Van Egeren et al. [11] showed by reconstructing the lineage histories of hematopoietic cells that the mutation might be acquired after birth and decades before disease onset. Watson et al. [12] obtained similar results using another approach. Currently, there are no results

available for $CALR^m$ patients.
Our inference method is proposed to study any kind of mutation, provided that some data are in accordance with those presented here for $JAK2^{V617F}$ and $CALR^m$ (see § D.1).

According to state of the art concerning the acquisition timing for the mutation $JAK2^{V617F}$, we choose to consider two hypotheses. Either T_0 is constant and equal to zero, or $T_0 > 0$ is a random acquisition time.
In the first case, we model the fact that the mutation would occur during fetal life. With the second hypothesis, we study the possibility that the mutation occurs after birth, during the course of life, assuming that T_0 follows an exponential law $\mathcal{E}(\lambda^{-1})$ of rate $1/\lambda$ (i.e. $\mathbb{E}[T_0] = \lambda > 0$ is the mean acquisition time of the mutation), this latter being an additional parameter to estimate.

A.4 Parameters and prior distributions

Table A.1 lists all model parameters with their associated values or prior distributions. Parameters are not defined at an individual (patient) level but at the level of a population of patients (either $JAK2^{V617F}$ patients or $CALR^m$). Heterogeneity between patients is thus assumed to result from the stochasticity of the model. The posterior distributions we will estimate for each population also account for this intra-population heterogeneity.

Parameter	Value	Prior	Reference
N_{WT}	10^5	-	Lee-Six et al. [6]
α	To estimate	$\sim \begin{cases} \text{Gamma law} \\ \text{with mean value} = 1/30\ [\text{days}^{-1}] \\ \text{with coefficient of variation} = 0.1 \end{cases}$	Mosca et al. [8]
(p_0, p_2)	To estimate	$\sim \begin{cases} \mathcal{U}([0,1]^2) \\ 0 \leq p_0 \leq p_2 \\ p_0 + p_2 \leq 1 \end{cases}$	-
p_1	$p_1 = 1 - p_2 - p_0$	$\in [0,1]$	-
Δ	$\Delta = p_2 - p_0$	$\Delta \geq 0$	-
q	$q = p_0/p_2$	$q \leq 1$	-
λ	To estimate	$\lambda \sim \begin{cases} 0 & \text{w.p } 0.5 \\ \mathcal{U}([0,100])\ [\text{years}] & \text{w.p } 0.5 \end{cases}$	[14, 11]
k_m	$\begin{cases} 7.5 \quad \text{for} \quad JAK2^{V617F} \\ 5.0 \quad \text{for} \quad CALR^m \end{cases}$	-	Mosca et al. [8]

Table A.1: List of the model parameters. For each of them, we indicate their value, or how they are related to each other, or "To estimate". In this latter case, we indicate the prior distribution they follow. $\mathcal{U}$ indicates a uniform distribution. "w.p" means "with probability".

In our model implementation, we consider p_0 and p_2 that can vary between 0 and 1, according to some constraints. Yet, we prefer considering Δ and q as our model parameters since they convey more biological meaning.
For parameter α - which models the rate at which mutated HSCs are recruited to divide - we choose a strong prior, so that α takes values around $1/30$ [days^{-1}] in a consistent manner with our previous results (Mosca et al. [8]). Actually, we could also have set this parameter constant. We choose a probability distribution defined on $\mathbb{R}_+^*$, here a gamma law (but other choices could have been possible), with a coefficient of variation (COV) small enough only to study how slight variations of this parameter

(around its mean) could potentially influence our results. Note that we also tested different COV and ended up with similar results.
For parameter λ, we consider *a priori* a zero-inflated prior distribution, where the prior probability that $\lambda = 0$ is set equal to 0.5, and otherwise λ is uniformly distributed over [0,100] [years]. $\lambda = 0$ might be considered an abusive notation. Actually, if $\lambda = 0$, then we do not sample - for each patient of the considered population - $T_0 \sim \mathcal{E}(\lambda^{-1})$, but rather consider that $T_0 = 0$. That is, $\lambda = 0$ corresponds to the hypothesis of mutation acquisition in the fetus while $\lambda > 0$ corresponds to the hypothesis of a mutation acquisition over life. This problematic of parameter estimation with a prior zero-inflated distribution is equivalent to a problematic of model selection, where our two models would be defined as $\{T_0 = 0\}$ (acquisition in fetal life) and $\{T_0 > 0\}$ (acquisition over life). More details about the actual implementation are given in § B.4.

B Parameter Estimation

B.1 ABC-SMC Procedure

For the estimation of the model parameters, we consider a Bayesian framework.
Let $\mathcal{D} = (\hat{t}_i, \hat{\eta}_i)_{i\in\{1,\cdots,N_p\}}$ be our N_p observations (CF $\hat{\eta}_i$ among progenitor cells at time $\hat{t}_i$ for individual i from one of the two considered patient populations: either $JAK2^{V617F}$ or $CALR^m$) and θ the random parameter vector to estimate. Our goal is to estimate the posterior distribution of θ given the data $\mathcal{D}$:

$$p[\theta|\mathcal{D}] \propto p[\mathcal{D}|\theta]\ p[\theta] \tag{4}$$

Since it is infeasible to obtain an analytical expression of the likelihood with our model, we have to use a likelihood-free estimation method. We will then approximate our posterior distribution using an Approximate Bayesian Computation based on Sequential Monte Carlo (ABC-SMC) in which the posterior distribution is obtained by iterative rejection sampling, with a decreasing sequence of tolerances [10, 1, 7]. This method is based on the simulation of the stochastic process and its comparison to the data.
Our model was implemented using the programming language Julia (and available on GitLab[1]). The ABC-SMC framework used to calibrate the model is available on GitLab at the following link:
https://gitlab-research.centralesupelec.fr/2017bentrioum/markovprocesses.jl.

All our estimations were computed using 2 000 particles. For each particle, we simulate as many trajectories (that do not drive to extinction) as observations. Each trajectory j gives us the number of mutated HSCs $N_j(t)$ over time. Using equation (2), we get the trajectories $\eta_j(t)$ of the clonal fractions among immature progenitor cells. We assign each trajectory to one and only one observation $(\hat{t}_i, \hat{\eta}_i)$ using an optimal affectation procedure based on the Hungarian algorithm [9, 5], minimizing a quadratic error between the trajectories and our observations (see § B.3). The final distance we compute is the averaged L2-norm between all our trajectories and the observations.
We progress from one step to another by choosing as next tolerance the median computed over the previous step.
Note that these computations are very heavy and were run on 250 processors in parallel on an HPC cluster.
We stop the algorithm when the procedure does not progress to the next step in less than 6 hours, with 250 processors (see Fig. B.1). We then look at the evolution of the L2 distance (Fig. B.2) and verify the algorithm's convergence by looking at the evolution of the posterior distribution of our parameters over the last steps (Fig. B.3). Finally, we also run the ABC-SMC procedure a second time with another random seed to ensure that we get the same results in both calculations. Both for the $JAK2^{V617F}$ and the $CALR^m$ datasets, 17 steps allows a proper convergence to the posterior distribution, as presented in Fig. B.3. That is, in the $CALR^m$ case, we run our computations until we reach a final tolerance equal to 0.0021, and in the $JAK2^{V617F}$ case equal to 0.0038.
As we can see in figures B.1 and B.2, the computational cost to reach steps 16 and 17 is high when the gain of the approximation error is low. As shown in Fig. B.3, the procedure could reasonably be stopped at step 16 (both for $CALR^m$ and $JAK2^{V617F}$).

[1] https://gitlab-research.centralesupelec.fr/2012hermangeg/mpn-development

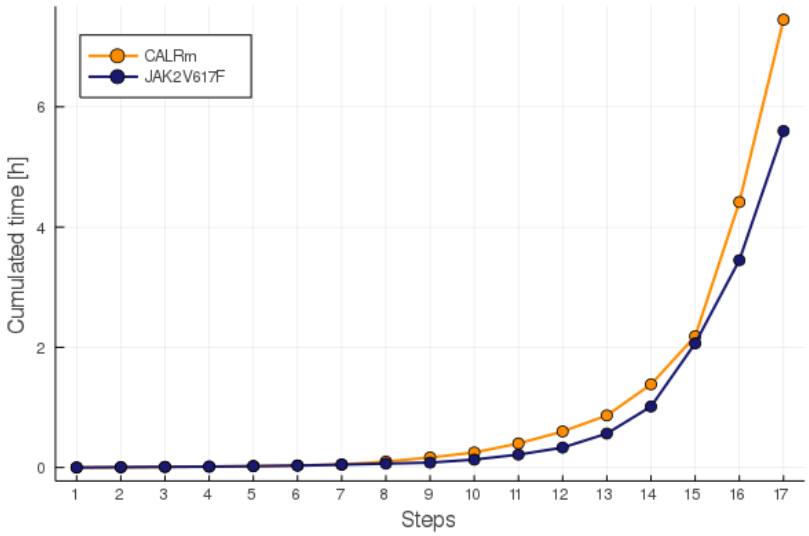

Figure B.1: Cumulated time (in hours) required for the ABC-SMC procedure to progress over the steps (with 250 processors used in parallel) in the $JAK2^{V617F}$ (blue) and $CALR^{m}$ (orange) cases.

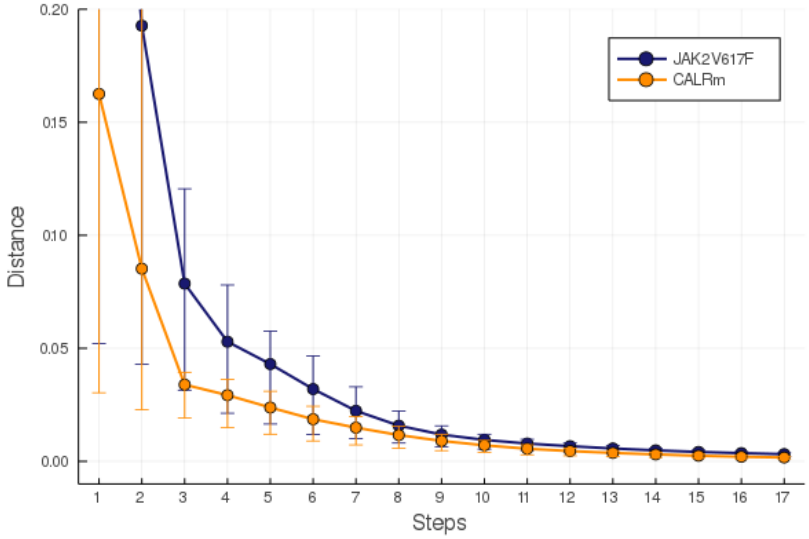

Figure B.2: L2-norm (distance) over the number of steps used for calibrating the model in the $JAK2^{V617F}$ (blue) and $CALR^{m}$ (orange) cases. Points are the mean distances computed over the 2 000 particles. Error bars represent a 90% confidence interval. For clarity, we truncated the y-axis.

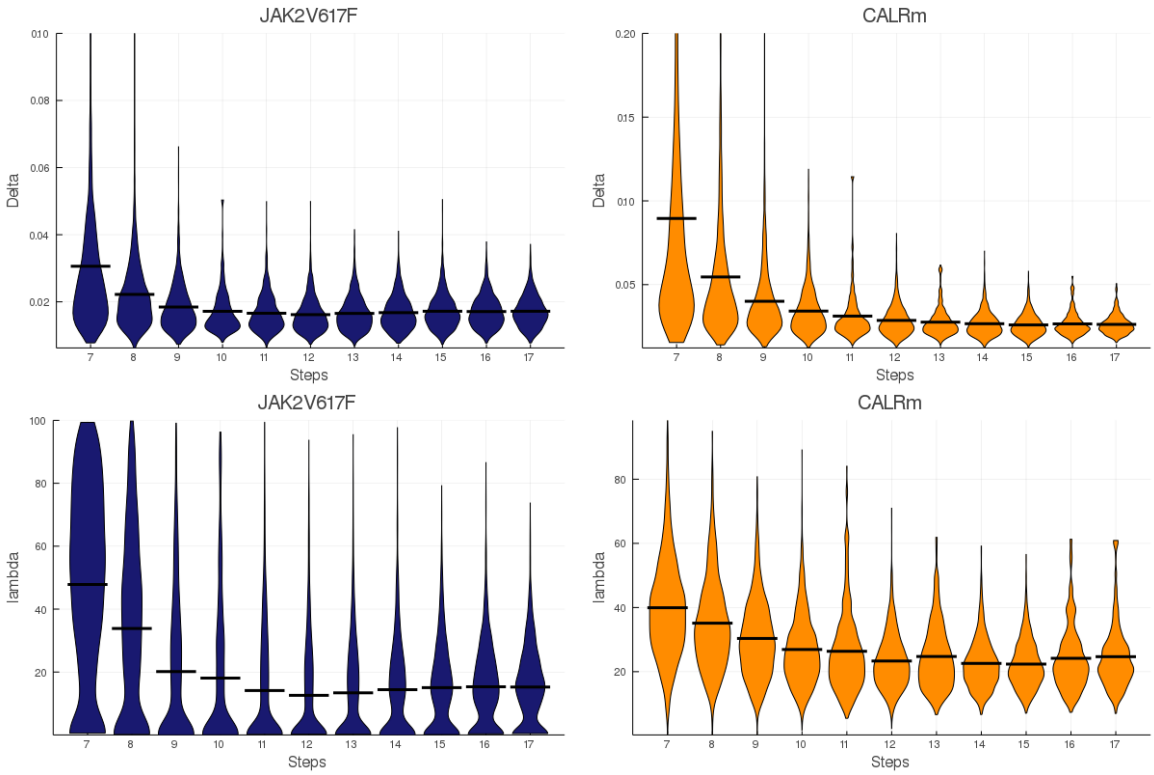

Figure B.3: Posterior distributions of parameters Δ (top) and λ (bottom) for the $JAK2^{V617F}$ (left) and $CALR^m$ (right) patient populations over the steps. x-axis begins at step 7 for clarity. Horizontal lines indicate mean posterior values.

B.2 Deterministic approximation

Our stochastic model is well suited to describe the expansion of a malignant clone from a single mutated cell. Indeed, when the number of mutated cells is low, stochastic effects play a crucial role (Fig. B.4).

When the number of cells becomes high, the stochastic formalism remains valid, but its simulation becomes more challenging. Our model is described by a CTMC. With our framework, basically, a trajectory is simulated by successively computing the time at which the next division of a mutated HSC occurs (what we call one iteration). The more mutated cells we have, the shorter is the time between two consecutive divisions. Then, when the malignant clone size becomes too important, it takes a huge number of iterations for the simulation to progress. This numerical difficulty is illustrated in figure B.5. We simulated two trajectories, setting for the parameter values $\alpha = 1/30$, $\Delta = 0.02$ and $p_2 = 0.03$, until they reach the number of $5 \cdot 10^5$ mutated HSCs. Knowing that we consider the expansion of a malignant clone in a stem cell pool of 10^5 wild-type HSCs, $5 \cdot 10^5$ mutated HSCs would be consistent with observations for $CALR^m$ patients where many measures of clonal fractions among progenitor cells exceed 80%. The dynamics of the malignant clone expansion for these two trajectories is shown on the left of Fig. B.5. Within the 30 first years, the expansion of the malignant clone is barely perceptible and then the number of cells quickly increases within a short period of time.

On the right of Fig. B.5, we look at the number of iterations required to simulate these two trajectories. A reasonable number of iterations is needed to simulate the expansion within the first decades, when the number of mutated HSCs is not too high, but then it becomes almost impossible to simulate the process until 58 years old, which is the median age in our cohort of $CALR^m$ patients (Tab. D.2).
Thus, it would be impossible to base our model calibration (that requires the simulation of many trajectories) purely on this stochastic process.
As observed in figure B.5 (left), when considering a huge number of cells, the stochastic effects are

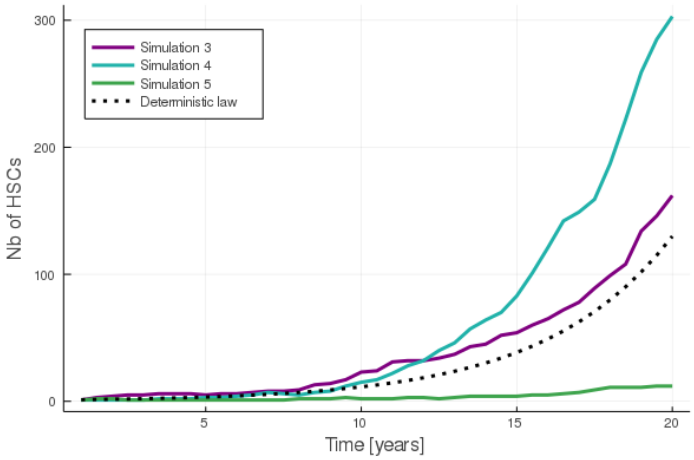

Figure B.4: Comparison between 3 simulations and the deterministic approximation when the process starts with one mutated HSC ($N_c = 1$). The parameter values used for the simulations are $\alpha = 1/30$, $\Delta = 0.02$ and $p_2 = 0.03$.

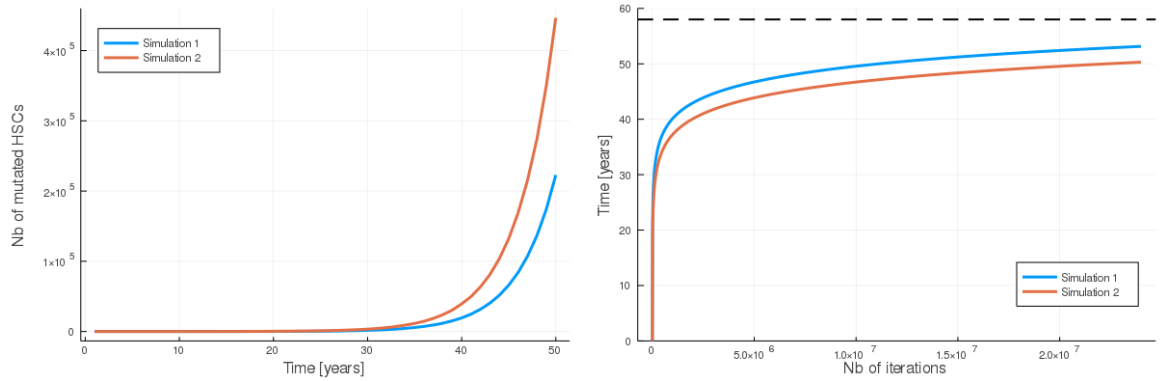

Figure B.5: Simulation of two trajectories with $\alpha = 1/30$, $\Delta = 0.02$ and $p_2 = 0.03$. On the left, increase of the number of mutated HSCs over time. On the right, number of iterations required so that the trajectories progress over time. The black dash horizontal line represents the median age among $CALR^m$ patients.

not visible and the clonal expansion looks exponential. Indeed, when a high number of cells N_c is reached at time t_c, then the dynamics of the clonal expansion at time $t > t_c$ will be very close to the conditional mean of the stochastic process:

$$\mathbb{E}[N(t)|N(t_c) = N_c] = N_c \exp\left(\alpha\Delta(t - t_c)\right) \tag{5}$$

Of course, this deterministic approximation cannot replace our stochastic model, as illustrated in Fig. B.4 and is actually not valid when N_c is too low.

Our objective is to determine a value for N_c such that the previous deterministic law (5) could be used without making a too large approximation error and that would not depend on the parameter values that are chosen. Such criterion is hard to obtain theoretically. Some authors have explored the question [2], but, in practice, the choice of a relevant value for N_c would be a compromise between an approximation error and a gain of computation time. That is why we choose to determine it empirically.

First, we consider the same parameter values as used previously. We simulate several trajectories starting with N_c mutated cells. We test 20 different values for N_c:

$$N_c \in \{1, 2, 5, 10, 20, 30, \cdots, 3\ 000, 4\ 000, 5\ 000\}$$

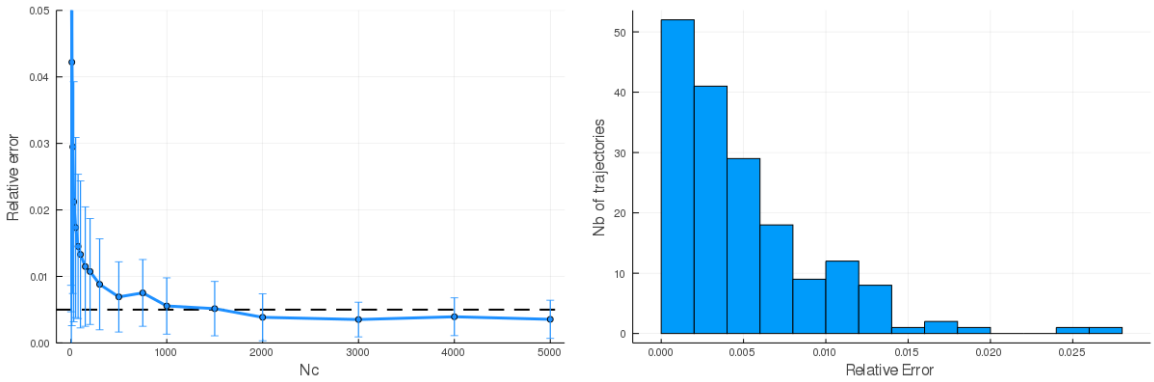

Figure B.6: Relative error between the deterministic approximation and realizations of our stochastic process. The errors are computed based on the time required to reach $N_{up} = 5 \cdot 10^5$ mutated HSCs. On the left, the error is a function of the initial number of mutated HSCs N_c for a given set of parameter values. The error bars represent standard deviations. The horizontal line represents a relative error of 0.5%. On the right, N_c is set equal to 2 000 and we represent the distribution of the relative errors for 175 trajectories whose parameters are randomly sampled from our prior distribution

and for each of them compute 100 simulations until $N_{up} = 5 \cdot 10^5$ cells are reached (restarting the simulations in case of extinction). Each trajectory will represent the clonal expansion from N_c to N_{up} mutated HSCs over a period of time of many years. The time needed to reach this upper bound N_{up} is a random variable. It can be compared to the deterministic time that it would take to reach this level with the deterministic approach:

$$T_{det} = \frac{1}{\alpha\Delta} \log\left(\frac{N_{up}}{N_c}\right) \tag{6}$$

If N_c is chosen high enough, then the error (relative to the deterministic value) would be low. In figure B.6 (left) we show that this error is decreasing with N_c. For $N_c = 2\,000$, the mean relative error goes below 0.005 and then decreases only slowly with higher values of N_c. Consequently, $N_c = 2\,000$ seems a valid criterion: above this number of cells the deterministic law is a good approximation of our process for the set of parameter values that we have chosen.
But the parameter values are not known in advance since our aim is to estimate them. We therefore have to check if this criterion remains valid for other parameter values. For that purpose, we sample parameter values according to our prior distribution and simulate trajectories from $N_c = 2\,000$ to $N_{up} = 5 \cdot 10^5$ mutated cells and evaluate the relative error as previously. As presented on the right of Fig. B.6, this criterion remains valid for different parameter values.
This choice is on the cautious side and might be sub-optimal, but it is sufficient to allow efficient enough simulation of trajectories so that we could run our ABC-SMC procedure within a reasonable time.

B.3 Optimal assignment

In the ABC-SMC procedure described in B.1, one simulation consists of sampling a parameter vector and computing as many trajectories (without extinction) as observations. Then, we assign one trajectory to one and only one observation and compute the quadratic error. Our distance is then the mean quadratic error. If this error is below the tolerance threshold, the parameter vector is rejected.
If N_p is our number of observations (and thus of trajectories), there would be $N_p!$ different possibilities for assigning one trajectory to one observation. Choosing the assignment randomly would not be a relevant choice. While theoretically convergent, it would highly depreciate the convergence speed of the procedure since it will result in a high rate of rejections. To circumvent this difficulty, we choose the optimal assignment such that the final mean quadratic error (computed over the N_p observations) is the lowest. Since computing all $N_p!$ possibilities would not be feasible, we use the Hungarian optimal affectation algorithm [5, 9] whose time complexity is $O\left(n^3\right)$.

B.4 Model selection or zero-inflated distribution for parameter λ

The age at which the mutation to the gene *JAK2* appears is subject to controversy, and there is a lack of study concerning the mutation to the gene *CALR*. This lack of knowledge justifies the use of mathematical models to test both hypotheses: either the mutation occurred during fetal life or was acquired after birth. In our model, both scenarios differ only by the way T_0 is modeled, either constant and equal to zero for all patients in the first case or a random variable following an exponential law with the additional parameter $\lambda > 0$ in the second case (see § A.3). The scenario of occurrence in fetal life can thus be considered as the limiting case of acquisition following an exponential law $\mathcal{E}(\lambda^{-1})$ when $\lambda = 0$. Then, discriminating between both hypotheses would be equivalent to evaluating when $\lambda = 0$ *vs* $\lambda > 0$. This implies allowing λ to be equal to zero with a non-zero probability, that is, choosing a zero-inflated law as prior distribution. In practice, this is implemented by using a binary parameter $\beta \in \{0, 1\}$, with prior probabilities $\mathbb{P}[\beta = 0] = \mathbb{P}[\beta = 1] = 0.5$, and a parameter l beeing *a priori* uniformly distributed over [0, 100] (years). In our ABC-SMC procedure, when parameter β is equal to zero, the mutation acquisition time T_0 is set to zero for all patients. On the other hand, if $\beta = 1$, we randomly sample as many acquisition times as there are individuals in the cohort, sampling them according to an exponential law $\mathcal{E}(l^{-1})$ of parameter $l > 0$. Finally, the posterior distribution of λ is retrieved from the samples of $\lambda = \beta\ l$.
This procedure is equivalent to considering two distinct models: if $\beta = 0$, we use the model of mutation acquisition in fetal life, while if $\beta = 1$, we use the model of occurrence over life.

C Simulation-based study of the model

C.1 Inference from synthetic data

When we design mathematical models to describe biological phenomena and want to identify them from experimental data, an important step is to first validate the practical identifiability of the model [13] and the consistency of our estimation methodology. It can be done using synthetic datasets generated from the mathematical model, and thus for which the ground truth is known. Especially, an important question is to know to which extent the number of available observations is sufficient to get robust conclusions from the model estimation.
In this article, we study two different hypotheses (or models) - $\lambda = 0$ *vs* $\lambda > 0$ - that we want to discriminate based on the observations of a limited number of patients. We also aim to interpret the estimated parameters since they carry relevant biological information.

N_i	Ground truth				Estimated parameters		
	Δ	q	λ	$\bar{T}_0$	$\hat{\Delta}$	$\hat{q}$	$\hat{\lambda}$
15	0.030	0.850	20.0	19.2	0.027	0.904	17.6
					$[0.018, 0.037]$	$[0.781, 0.956]$	$[10.3, 27.3]$
15	0.023	0.850	0.0	0.0	0.020	0.924	0.2
					$[0.016, 0.024]$	$[0.815, 0.963]$	$[0, 3.8]$
14	0.139	0.554	0.0	0.0	0.146	0.604	0.0
					$[0.112, 0.184]$	$[0.285, 0.767]$	$[0, 0]$
11	0.092	0.817	55.9	35.5	0.098	0.658	32.5
					$[0.056, 0.166]$	$[0.223, 0.861]$	$[17.4, 53]$
15	0.119	0.336	38.2	19.4	0.127	0.612	21.3
					$[0.08, 0.193]$	$[0.244, 0.817]$	$[12.1, 33]$
12	0.021	0.939	37.7	21.8	0.021	0.912	25.1
					$[0.014, 0.028]$	$[0.784, 0.966]$	$[13.4, 41.1]$
14	0.197	0.546	96.6	40.1	0.058	0.786	41.3
					$[0.036, 0.085]$	$[0.488, 0.913]$	$[23.3, 65.1]$
12	0.366	0.330	0.0	0.0	0.368	0.285	0.0
					$[0.284, 0.462]$	$[0.045, 0.481]$	$[0, 0]$
15	0.134	0.664	0.0	0.0	0.142	0.618	0.0
					$[0.11, 0.179]$	$[0.328, 0.767]$	$[0, 0]$
14	0.027	0.945	36.1	16.4	0.032	0.869	20.2
					$[0.022, 0.045]$	$[0.672, 0.947]$	$[11.5, 31.4]$
12	0.251	0.427	0.0	0.0	0.247	0.382	0.0
					$[0.203, 0.294]$	$[0.068, 0.61]$	$[0, 0]$

Table C.1: Results of the parameter estimation procedure using synthetic data. N_i observations are generated from the model with known parameter values (ground truth). The model parameters are then estimated using the ABC-SMC procedure (estimated parameters). We report the mean posterior values of Δ, q, and λ parameters and 95% credibility intervals. We omit for clarity parameter α since it does not much deviate from its prior. For the ground truth values, we also indicate $\bar{T}_0$, which is the mean "observed" acquisition time over the N_i simulated trajectories.

We generate different datasets. For each of them (index i), we sample a parameter vector θ_i (ground truth) and simulate N_i trajectories from our model. N_i is chosen randomly between 11 (number of $JAK2^{V617F}$ patients we have in our real dataset) and 15 (number of $CALR^m$ patients). For each trajectory (indexed by $j \in \{1, \cdots, N_i\}$), we sample a value y_j between 0 and 1. Our observation time and observed clonal fraction $(\hat{t}_j, \hat{\eta}_j)$ are determined such that $\eta(\hat{t}_j) = y_j = \hat{\eta}_j$ (with the function η given in Equation (1)). We only consider trajectories without extinction and observation time $\hat{t}_j \in [0, 100]$ years. If one of these two conditions is not respected, we simulate a new trajectory until satisfying both constraints. We define $\bar{T}_{0,i} = \frac{1}{N_i} \sum_{j=1}^{N_i} T_{0,i,j}$ the mean "observed" acquisition time over the N_i

simulated trajectories.
Then, we run our parameter estimation procedure until convergence and compare our estimated parameters (mean posterior values and 95% credibility intervals) with the actual values used to generate the data. Results of this study are presented in Tab. C.1.
Parameters Δ and q are well estimated overall. We also correctly retrieved if data were generated according to the hypothesis of mutation acquisition in fetal life ($\lambda = 0$, i.e, $T_0 = 0$) or that of an occurrence over life ($\lambda > 0$, i.e, $T_0 > 0$). Yet, in the case of an acquisition after birth, λ is not very well estimated. But if we consider, instead of λ, the mean "observed" acquisition time $\bar{T}_0$ (let us recall that $T_0 \sim \mathcal{E}(\lambda^{-1})$ such that $\mathbb{E}[T_0] = \lambda$) computed over the N_i simulated trajectories, we find that $\hat{\lambda}$ estimates with accuracy $\bar{T}_0$. In our simulated dataset, the difference between $\bar{T}_0$ and λ is explained by the fact that we simulate censored observation times[2]. Indeed, to have a synthetic dataset consistent with real observations, we enforce that the observation time is below 100 years. Then, for large values of λ, trajectories with late acquisition times are automatically excluded from our dataset, therefore $\bar{T}_0 < \lambda$. Consequently, our estimation of λ might be potentially biased. We explore this point in more detail in the next paragraph.

[2]Without censoring, we would have $\lim_{N_i \longrightarrow \infty} \bar{T}_0 = \lambda$

C.2 Bias in the estimation of λ

Our observations are censored: individuals who would acquire the driver mutation at too old an age would not appear in our cohort since they would die before exhibiting MPN symptoms and before having too high CF.
In our model, λ is the mean mutation acquisition time, estimated from censored observations. Thus, instead of truly estimating λ, we estimate the mean "observed" acquisition time $\bar{T}_0$, as shown in the previous paragraph. Intuitively, if the true value for λ is low, it can still be accurately estimated since it will effectively correspond to the mean "observed" acquisition time. If too high, the mean "observed" acquisition time over the population $\bar{T}_0$ would be such that $\bar{T}_0 < \lambda$ and parameter λ would be underestimated. We quantify this effect of censoring on estimation with a simulation-based study.

For $\lambda \in \{1, 2, \cdots, 100\}$, we repeat for $i \in \{1, \cdots, 1000\}$ the following procedure:

- We sample a parameter vector θ_i from our prior (except λ that is assigned to a given value)
- We simulate 15 trajectories (without extinction), $j \in \{1, 2, \cdots, 15\}$
- We keep track of the 15 acquisition times $T_{0,i,j}$
- For each trajectory j, we sample a value uniformly between 0 and 1 for the CF $\eta_{i,j}$, and compute the associated observation time $t_{i,j}$
- We censor the individuals (trajectories) whose observation time $t_{i,j}$ exceeds 100 years. We get $N_i \leq 15$ uncensored trajectories.
- We compute the mean "observed" acquisition time $\bar{T}_{0,i}$ (computed over the N_i uncensored trajectories)

Then we compute the mean (over the 1,000 iterations) number of censored individuals (trajectories) over the 15 simulated trajectories for each $\lambda \in \{1, 2, \cdots, 100\}$ (Fig. C.1). We observe that, for $\lambda \geq 25$, the censoring effect begins. The higher the true λ, the higher the number of censored individuals.

We also compute, for each $\lambda \in \{1, 2, \cdots, 100\}$, the mean (over the 1,000 iterations) "observed" acquisition time $\bar{T}_0$ (calculated over the uncensored individuals) and the 5 and 95% quantiles (Fig. C.2). For $\lambda < 20$ years, there is not much difference between λ and $\bar{T}_0$. Then, we progressively observe the effect of censoring individuals (trajectories). With our parameter estimation procedure, we estimate accurately $\bar{T}_0$ rather than the true λ (as shown in the previous section). In the $JAK2^{V617F}$ case, where we estimated pretty low values for λ (with a mean value of approximately 15 years), we are in the range of values where we should estimate it accurately. For the $CALR^m$ case, for which we estimated a mean value of λ about 25, we likely underestimated the true acquisition time. With our simple model of censoring, estimating an acquisition time of 25 years (that would thus correspond to $\bar{T}_0$) might approximately correspond to an actual acquisition time of about 28 years (corresponding to the true value of λ).
This study has two primary limits: first we consider a censoring age of 100, when a more accurate analysis would account for more realist demographic values. Second, the CF fraction is uniformly sampled over [0,1], when a more thorough study would account for a distribution of these CF values more in line with those found in reality. Yet, even with this simplistic model of censoring, we can find some qualitative results, namely that we probably slightly underestimate the actual acquisition time of the mutation $CALR^m$ for the general population. Then, our estimate for parameter λ should be considered as the estimated mean acquisition time of the mutation for the individuals that will develop an MPN, and they are actually the individuals that we focus on in our study.

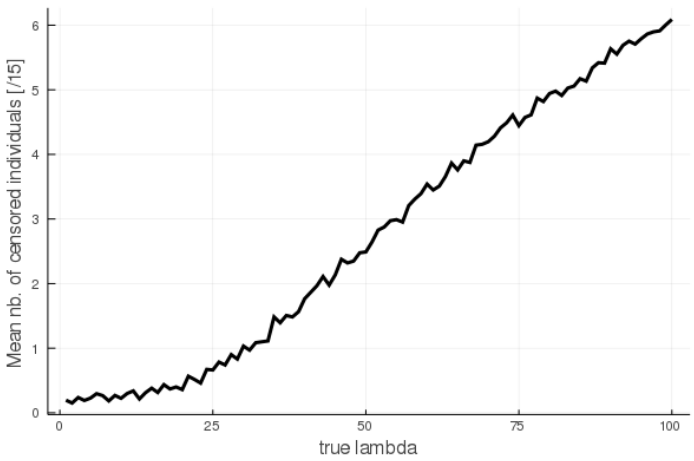

Figure C.1: Number of censored individuals (observation times higher than 100 years) for a simulated cohort of 15 individuals, for different values of λ (mean value calculated on 1,000 simulations for each value of λ).

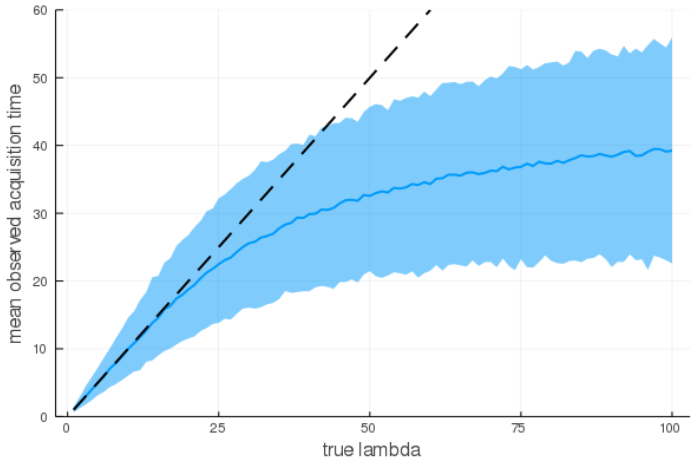

Figure C.2: Mean "observed" acquisition time $\bar{T}_0$ computed for uncensored individuals (y-axis) against the true mean acquisition time λ (x-axis) of the mutation. Blue line indicates the mean value (for each true λ, $1,000 \times 15$ trajectories are simulated) and shaded area represents a 90% confidence interval. Dashed black line materialises $\bar{T}_0 = \lambda$.

C.3 Robustness of the estimation of Δ

In our model-based study on the development of MPN, we made the following assumptions:

- A constant value of Δ over the lifetime
- A constant number of WT HSCs

We will illustrate in the following how violations of these assumptions might impact our estimation of Δ.
To simplify, we will consider the case of a mutation acquired in fetal life (that is, $T_0 = 0$, or equivalently, $\lambda = 0$) and study the dynamics of the clonal expansion described by the deterministic approximation (5), that is:

$$N(t) = \exp(\alpha \Delta t)$$

We set $\alpha = 1/30$ [/days] and $\Delta = 0.02$ (the same values as used in § B.2)

C.3.1 Variable Δ over the lifetime

An expanding malignant clone (with one initial driver mutation) can acquire an associated mutation also impacting hematopoiesis over the lifetime, resulting in two subclones: one without the associated mutation and one with it. We suppose that this latter subclone has a greater proliferative advantage. Thus, if we only look at the driver mutation, that is, disregarding whether or not the associated mutation is present, we might overestimate the proliferative advantage of the driver mutation since our observation also includes the information about an associated mutation. We illustrate this point in the following example.
We consider a malignant clone (with the initial driver mutation) that expands at a rate of $\alpha\Delta$. We consider that one mutated cell of this clone acquires an associated mutation at time $t = 20$ years, resulting in two subclones: one with only the driver mutation that continues to expand at a rate $\alpha\Delta$, the second with the associated mutation that will develop at a growth rate $\alpha\Delta(1 + z)$ with $z > 0$. Here, we choose $z = 1$ (Fig. C.3).

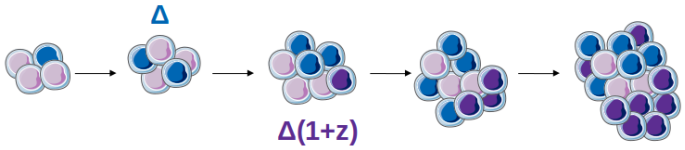

Figure C.3: Schematic representation of the clonal expansion of a malignant clone with one driver mutation (blue cells), whose proliferative advantage is Δ. At some point, one mutated cells acquires an associated mutation (purple cell), that confers to it an higher proliferative advantage $\Delta(1 + z)$. Then, two subclones expand in parallel, with different growth rates.

Figure C.4 (top panel) shows the number of mutated cells according to whether or not the (sub)clone presents the associated mutation. In the first years following the associated mutation, the subclone having only the driver mutation remains the main one: the subclone with the associated mutation would be barely perceptible during this period (Fig. C.4, middle panel). Then, there is a period during which both subclones coexist, each with non-negligible CF. Eventually, the subclone with the associated mutation will take over.
Without the information about the associated mutation, we would measure the CF of both subclones together. From this observation, we would infer the value for Δ (Fig. C.4 bottom panel). In this illustrative example, when the associated mutation is barely perceptible, the estimated value for Δ would be that of the initial clone. Then, when both subclones coexist, we slightly overestimate this parameter. Yet, even when one subclone takes over, we are far from estimating the proliferative

advantage of the subclone with the associated mutation.
This qualitative study shows that the proliferative advantage of the driver mutation (either $JAK2^{V617F}$ or $CALR^{m}$) could be slightly overestimated because of patients having associated mutations (see § D.1). However, the acquisition of mutations in "WT" cells (which should not be considered WT anymore) could also compensate for the effect. We study this latter point in the next paragraph.

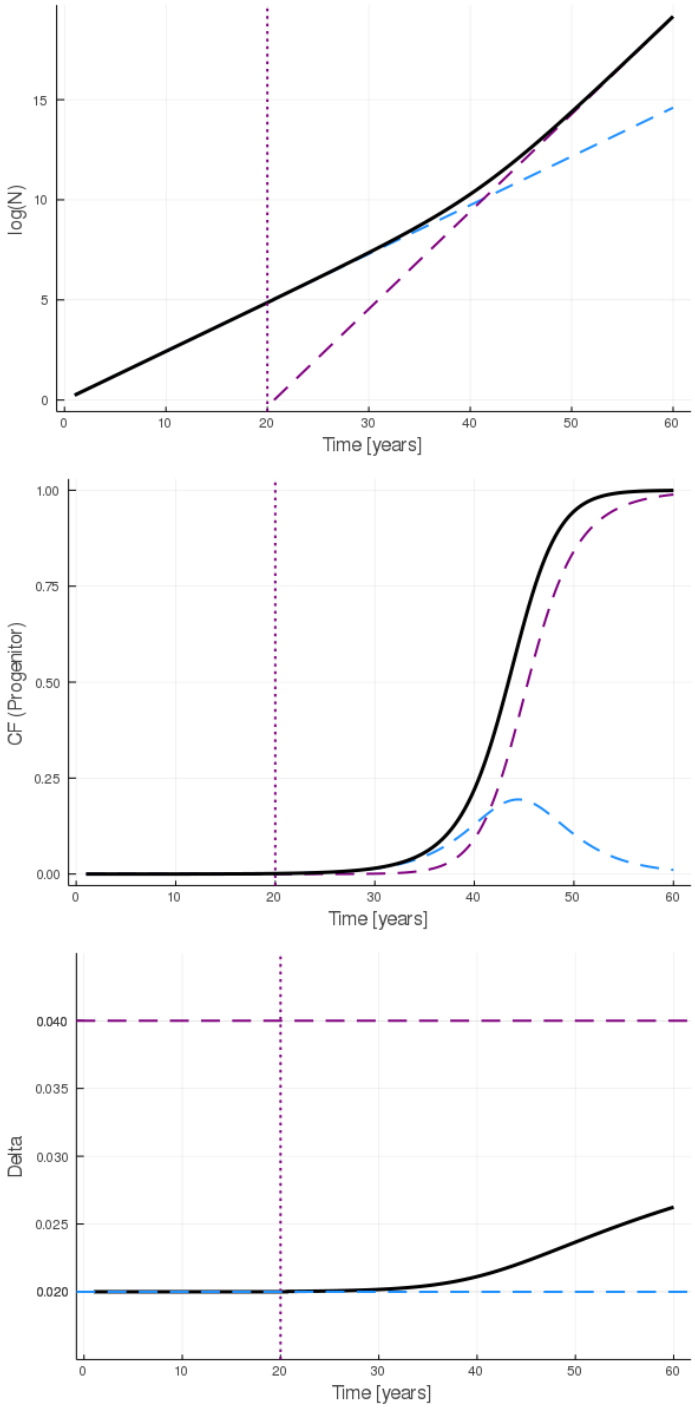

Figure C.4: Dynamics of two subclones: the first one (blue line) having only the driver mutation (with a proliferative advantage $\Delta = 0.02$), and the second one appeared at $t = 20$ years (vertical purple dashed line) having an associated mutation which conferred to him a higher proliferative advantage $\Delta(1 + z) = 0.04$. The top panel shows the clonal expansion (log number of HSCs) of each subclone (blue and purple dashed lines) when the solid black line represents the number of both mutated cells (that is, mutated cells with the driver mutation, whether or not they also have the associated mutations). When, experimentally, we only search for the driver mutation, it corresponds to having the information for the black line (at a given time). The middle panel represents the CF that would be measured among progenitor cells. The bottom panel's black curve indicates what would be the theoretical estimated value of Δ when there are two subclones but that we only assume a clonal expansion of one clone. The objective would be to accurately estimate the proliferative advantage of the driver mutation ($\Delta = 0.02$, blue line). Still, because of the acquisition of an associated mutation, the value of Δ might be overestimated.

C.3.2 A variable number of WT HSCs during life

Our model assumes a constant number of WT HSCs equal to 100,000 [6]. Yet, the number of WT HSCs is not necessarily constant over the lifetime. WT cells can also acquire mutations in the *TET2* or *DNMT3A* genes, for example, so that they would not be really WT anymore. So, to be more precise, we should say that we study the expansion of a malignant clone with $JAK2^{V617F}$ or $CALR^m$ driver mutations parallel to HSCs that do not have this mutation. In our model, we assume this latter pool to be of constant size when it might actually also expand because of mutation acquisitions.
To illustrate this point, we consider a clonal expansion as described in previous paragraph; that is, we set $\Delta = 0.02$. Then, we consider that the number of WT HSCs (we continue to define them a bit abusively as WT; it would be more precise to consider them as not $JAK2^{V617F}$ or not $CALR^m$) increases, from an initial number of N_{WT}=100,000, at a rate $\alpha\Delta x$ with $x < 1$. We illustrate this dynamics in Fig. C.5 (top panel) with different values for x: 0.0 (as in the main model), 0.05, 0.1, and 0.2.
The expansion of the WT HSC pool will result in a reduced CF among progenitor cells $\tilde{\eta}$, compared to the situation with a constant number of HSC (η, given by eq. (2), when $x = 0$), as illustrated in Fig. C.5 (middle panel):

$$\tilde{\eta}(t) = \frac{1-\Delta}{1-\Delta+N_{WT}\exp(\alpha\Delta(x-1)t)} < \eta(t)$$

Then, if the previous equation describes the actual dynamics but we still model the WT HSC pool as being of constant size, we would estimate a reduced value $\tilde{\Delta} \approx \Delta(1-x)$, as illustrated in Fig. C.5 (bottom panel). If the malignant clone of interest has a much higher proliferative advantage than the ones for the mutations that occurred in WT cells (i.e, $x \ll 1$), we would only slightly underestimate the value Δ of the mutation.

The number of WT HSCs could also vary because of other factors, such as ageing. Lee-Six et al. inferred, based on phylodynamics methods and the data of a 59 years old healthy individual, the evolution of the HSC population size over life [6]. We report their findings (mean value) in Fig. C.6 (top panel) and now study how our estimation of Δ would be impacted if, instead of considering that $\log(N_{WT}(t))$ linearly increases over life, we consider the same evolution for $N_{WT}(t)$ as the one reported by Lee-Six et al. [6]. Results of this study are displayed in Fig. C.6 (bottom panel). Above 30 years, when the presence of mutated cells becomes perceptible in our illustrative example, sometimes we overestimate, sometimes we underestimate the true proliferative advantage $\Delta = 0.02$, depending on the evolution of the WT HSC pool size.

As a conclusion of this qualitative study, based only on limited examples, we see how more complex models that account for the acquisition of associated mutations in the malignant clone, acquisition of mutations in WT HSCs, or evolution of the WT HSC pool size over life, can impact our estimations of the proliferative advantage Δ of the diver mutation of interest (either $JAK2^{V617F}$ or $CALR^m$). When the acquisition of associated mutations in a patient might result in overestimating Δ, the increasing size of the WT HSC pool will have the reverse effect. If both occur, they might compensate in some ways. We should then consider that our estimation of parameter Δ also accounts for various effects over a lifetime that are impossible to enumerate in detail, even less quantify.
Our results remain therefore valid as long as these effects do not predominate over the expansion of the mutated clone, and that they would have the same order of magnitude for patients having the mutation $JAK2^{V617F}$ and those having the mutation $CALR^m$ (such that we could compare both populations). Note that, to respect this assumption, we excluded patients with homozygous mutated cells. Indeed, we could not reasonably assume that homozygous subclones have the same proliferative advantage than the heterozygous ones.
We should also highlight that parameter Δ is estimated at a population level, not for a given patient. When looking at the mutations in the population of $JAK2^{V617F}$ or $CALR^m$ patients, only some of them were found with associated mutations (note that patients with Essential Thrombocythemia display very few associated mutations); patients with more than one driver mutation might not bias our estimations to a too large extent.

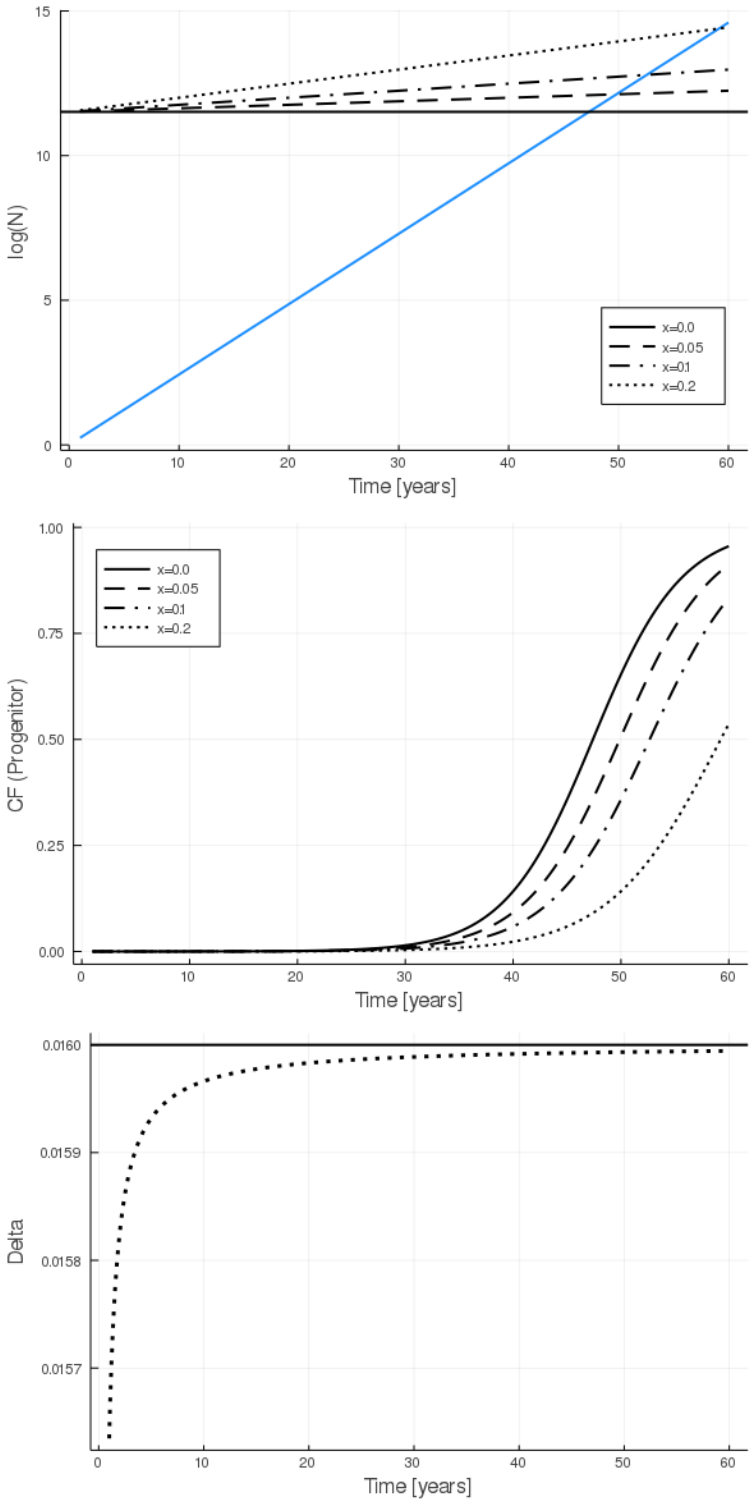

Figure C.5: Dynamics of the clonal expansion of a malignant clone when WT HSCs also expand. The top panel displays the increasing log-number of mutated HSCs (blue line) and the log-number of WT HSCs for different x-values (black lines). $x = 0$ corresponds to our model, with N_{WT} being constant. To these dynamics in the HSC pool correspond evolutions of the clonal fraction (CF) among progenitor cells, as displayed in the middle panel. An expansion of the WT HSC pool will result in reduced values for the CF of mutated cells, and, thus, underestimating the proliferative advantage Δ of the driver mutation. The bottom panel shows what would be the estimation of Δ (dotted line) if assuming a constant number of WT HSCs, when, in reality their pool would expand with $x = 0.2$. The horizontal line corresponds to $\Delta(1-x)$. When mutated cells are perceptible, we will underestimate Δ by a factor $(1-x)$.

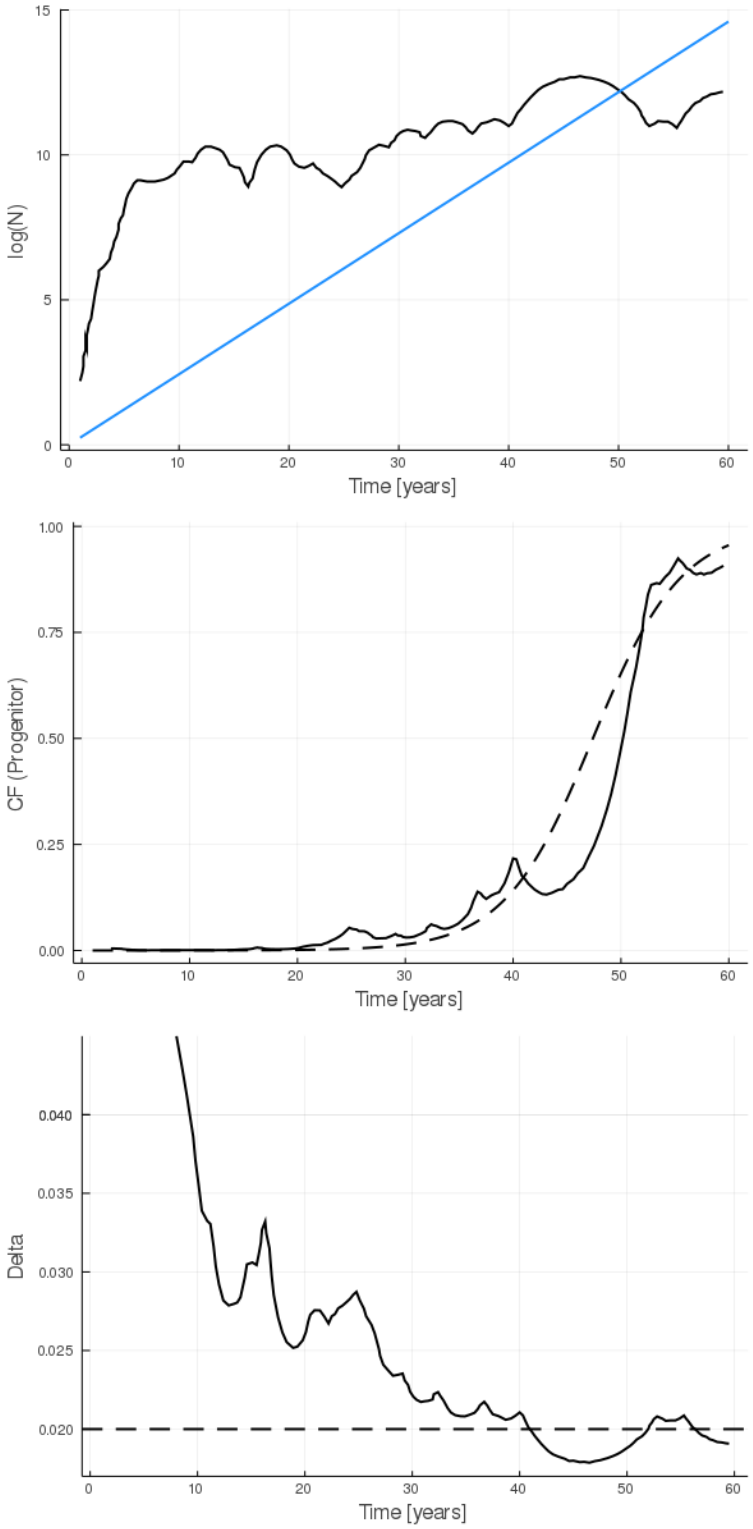

Figure C.6: The top panel presents the dynamics of the clonal expansion of a malignant clone (blue line) parallel to WT HSCs whose number vary over life according to Lee-Six et al. [6] (black line). y-axis are in a log-scale. The middle panel shows the evolution of the corresponding CF among progenitor cells (solid line) compared to the one that would be obtained from our model, assuming a constant number of WT HSCs equal to 100,000 (dashed line). The bottom panel shows what would be the estimation of Δ (solid line) if assuming a constant number of WT HSCs, when, in reality their pool expands according to the dynamics reported in [6].

D Estimations based on real data

D.1 Data

To estimate our model parameters, we use data from 15 $CALR^m$ [3] and 11 $JAK2^{V617F}$ (from Mosca et al. [8]) recently diagnosed MPN patients that have no homozygous mutated HSCs. Note that we conduct two separate model calibrations, first for $JAK2^{V617F}$ patients, then for $CALR^m$ ones. The clonal architectures of the hematopoietic progenitor and stem cells were measured before patients start a therapy. The extraction and purification of highly immature hematopoietic stem cells is very challenging, and it is infeasible to obtain information for true HSCs. Thus, the information we will consider in most cases - and when available - is the clonal fraction (CF, that is the fraction of mutated cells) of HSC-enriched progenitor cells ($CD90^+CD38^-CD34^+$). Let $(\hat{t}_i, \hat{\eta}_i)$ denote our observations where $\hat{\eta}_i$ is the CF of immature progenitor cells of patient i measured at age $\hat{t}_i$.
The observed CF $\hat{\eta}_i$ among immature progenitor cells is therefore an indirect measure of the number of mutated HSCs. We consider it as a realization of the stochastic process $\eta(t)$ at time $\hat{t}_i$ (see eq. (2)).

Tables D.1 and D.2 list the patients whose observations are used in this article. The CF corresponds to the measured heterozygous Clonal Fraction (in percentage) among the corresponding progenitor compartment. For $CALR^m$ patients, we also indicate the mutation type (T1 or T2), corresponding to the 2 most frequent variants in $CALR^m$ patients. We also give the information about other mutations found associated in the same or different HSCs. The information is obtained from VAF measures in mature cells; we cannot know whether the other mutations are present in subclones having the driver mutation ($CALR^m$ or $JAK2^{V617F}$), or not.
To verify $JAK2^{V617F}$ was not a germinal mutation, we purified and analyzed the $JAK2^{V617F}$ VAF in T lymphocytes from 8 out of 11 patients available (that is, all $JAK2^{V617F}$ patients except #3, #5, and #11). We did not detect the $JAK2^{V617F}$ mutation in those cells showing that they do not belong to the clone and that the mutation is acquired and not germline.
We only consider patients' observations before they started a therapy under IFNα. Furthermore, we do not consider patients with homozygous subclones, except for patients P4 and P28 that had respectively homozygous CF of 2% and 1.7%. Since these values were very low, we made the assumption that the homozygous mutated cells had a behaviour similar to the heterozygous ones and thus the CF considered in the table is the sum of the CF for homozygous and heterozygous cells.

The CF among progenitor cells were measured based on the surface markers CD34, CD38 and CD90 and cells were sorted according to the following phenotypes: $CD34^+CD38^+$, $CD34^+CD38^-CD90^-$ and $CD34^+CD38^-CD90^+$. Briefly, different progenitor cells were isolated from the other cells, purified and sorted at one progenitor per well in 96-well plates. Each progenitor gave a progeny of cells (colony) after 10 to 15 days of culture. The genotyping of each colony by Taqman allelic discrimination qPCR enabled to retrospectively know the genotype of each progenitor (more details previously reported by Mosca et al. [8] and El-Khoury et al. [3]).

ID	ID_0	Age	CF [%]	Progenitor compartment	Other mutations	Disease
1	P2	34	35	CD34+CD38-	None	PV
2	P4	58	70.5	CD34+CD38-CD90+	TET2fS1906Rfs (25%)	PV
3	-	39	5	CD34+CD38-CD90+	TET2 Y1679Pfs* (45%) DNMT3A N727D (20%)	ET
4	P11	51	50	CD34+CD38-	SUZ12 Ala33Val (61%)	PV
5	P14	35	5	CD34+CD38+CD90-	None	ET
6	-	57	14.5	CD34+CD38-CD90+	None	PV
7	P20	45	2	CD34+CD38-	None	PV
8	P22	53	19	CD34+CD38-CD90+	None	PV
9	-	29	17	CD34+CD38-CD90+	None	ET
10	-	61	32	CD34+CD38-CD90+	None	ET
11	P28	51	13	CD34+CD38-	None	PV

Table D.1: Observations for $JAK2^{V617F}$ patients (from Mosca et al. [8]). Age is in years. ID_0 refers to the label used in [8]. If ID_0 = "-", then the patient's data is used for the first time in our article. The information about other mutations - associated in the same or different HSCs than those carrying the driver mutation - is obtained from measures in mature cells. The percentage refers to a VAF measure. The last column indicates the disease of the patient. ET for Essential Thrombocythemia; PV for Polycythemia Vera.

ID	ID_0	Type	Age	CF [%]	Progenitor compartment	Other mutations	Disease
1	P166	1	48	30.4	CD34+CD38-CD90+	None	ET
2	P46	1	58	100	CD34+CD38-CD90+	None	ET
3	P30	1	70	91.8	CD34+CD38-CD90+	None	ET
4	P48	1	53	68.2	CD34+CD38-	TP53 V143M (7%)	ET
5	P90	1	58	7.7	CD34+CD38-CD90+	None	ET
6	P169	1	46	100	CD34+CD38-CD90+	None	ET
7	P38	1	66	100	CD34+CD38-CD90+	ASXL1 G658* (6%) ASXL1 E635Rfs (40%) EZH2 R690H (27%)	PMF
8	P157	1	44	50	CD34+CD38-CD90+	SF3B1 K666N (28%) JAK2V617F (2%)	PMF
9	P28	2	53	99.7	CD34+CD38-CD90+	None	ET
10	P54	2	49	100	CD34+CD38-CD90+	None	ET
11	P103	2	60	100	CD34+CD38-CD90+	None	ET
12	P53	2	69	24	CD34+CD38-CD90+	DNMT3A L901R (22%)	ET
13	P187	2	86	79	CD34+CD38-CD90+	ASXL1 L775fs* (2%)	PMF
14	P170	2	70	94	CD34+CD38-CD90+	None	ET
15	P52	2	44	5	CD34+CD38-CD90+	None	ET

Table D.2: Observations for $CALR^m$ patients [3]. Age is in years. ID_0 refers to the label used in [3]. We indicate whether the $CALR^m$ mutation is type 1 or 2. The information about other mutations - associated in the same or different HSCs than those carrying the driver mutation - is obtained from measures in mature cells. The percentage refers to a VAF measure. The last column indicates the disease of the patient. ET for Essential Thrombocythemia; PMF for Primary Myelofibrosis.

D.2 Posterior distributions for the real data

We run our ABC-SMC procedure until convergence (see § B.1) and get the parameter posterior distributions for the $JAK2^{V617F}$ patient population (Fig. D.2) and the $CALR^m$ one (Fig. D.3).

A key parameter of our model is $\Delta = p_2 - p_0$. It gives an indication on how important is the unbalance between symmetric and differentiated divisions that drives the clonal expansion of the mutation. For $CALR^m$ patients, we estimate as mean value $\Delta = 0.026$ (see Fig. D.3, top left), and for $JAK2^{V617F}$ patients, a mean value equal to 0.017 (see Fig. D.2, top left). Our results indicate that the mutation $CALR^m$ would give a higher proliferative advantage at the stem cell level than the $JAK2^{V617F}$ mutation, with notably $\mathbb{P}[\Delta > 0.017 \mid \mathcal{D}_{CALR^m}] = 0.99$.
The effect of the parameter Δ can be seen on the trajectories presented in Fig. D.1 and compared to the data. A higher value of Δ is directly responsible for the steeper increase of the mutated $CALR^m$ clonal fraction compared to $JAK2^{V617F}$.

Parameter λ refers to the mean acquisition time of the mutation in our model. Its prior distribution was chosen zero-inflated so that we allowed $\lambda = 0$ with a non-zero probability, this latter situation corresponding to the hypothesis of a mutation acquisition in fetal life.
In the case of the $JAK2^{V617F}$ patient population, the posterior distribution of λ is still zero-inflated with $\mathbb{P}[\lambda = 0.0 \mid \mathcal{D}_{JAK2^{V617F}}] = 0.24$ (Fig. D.2, bottom left), which is not the case anymore for the $CALR^m$ population where, for this latter, $\lambda > 0$ almost surely (Fig. D.3, bottom left). The posterior mean value of λ is equal to 15.2 years for $JAK2^{V617F}$ and 24.7 for $CALR^m$, suggesting a much later acquisition of the mutation $CALR^m$ compared to $JAK2^{V617F}$, with notably $\mathbb{P}[\lambda < 15.2 \mid \mathcal{D}_{CALR^m}] = 0.13$.

Parameter $q = p_0/p_2$ corresponds in our model to the probability of stochastic extinction of the process. Its mean posterior value is estimated at 0.87 and 0.94 for $CALR^m$ and $JAK2^{V617F}$ patient populations, respectively, with $\mathbb{P}[q > 0.94 \mid \mathcal{D}_{CALR^m}] = 0.25$ (see figures D.2 and D.3, top right). These estimations would be in line with what could be expected: a mutation that would appear in the population at a higher rate than the incidence rate of MPN. Note that, with our model, there are two situations in which an individual who acquires the mutation does not develop an MPN: either the malignant clone naturally disappears, or the mutation is acquired late in life so that the malignant clone does not have time to expand given its estimated expansion rate.

Lastly, we present on the bottom right of figures D.2 and D.3 the posterior distribution of parameter α that models the division rate of HSCs. Its posterior distributions do not deviate from the prior for the two populations.

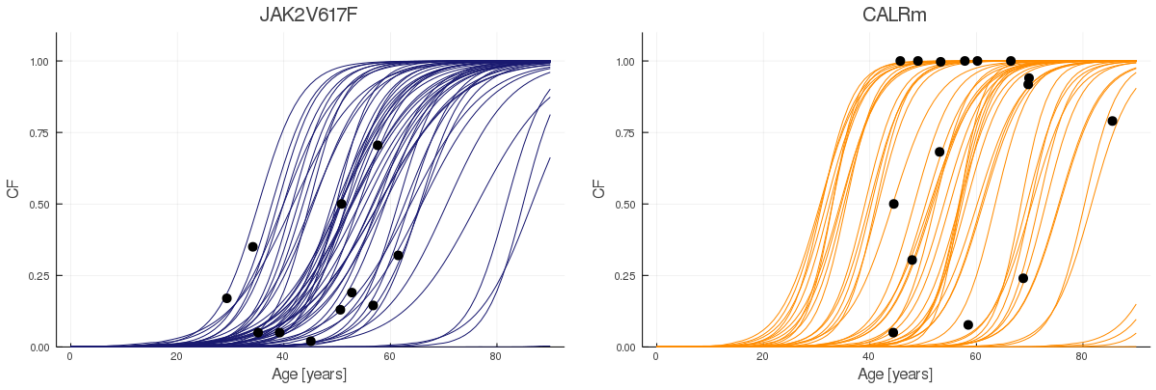

Figure D.1: Confronting $JAK2^{V617F}$ (left) or $CALR^m$ (right) patient observations (black points) to 50 trajectories simulated with the model and parameters sampled from the posterior distributions (colored solid lines) and representing the evolution of the CF among progenitor cells with age.

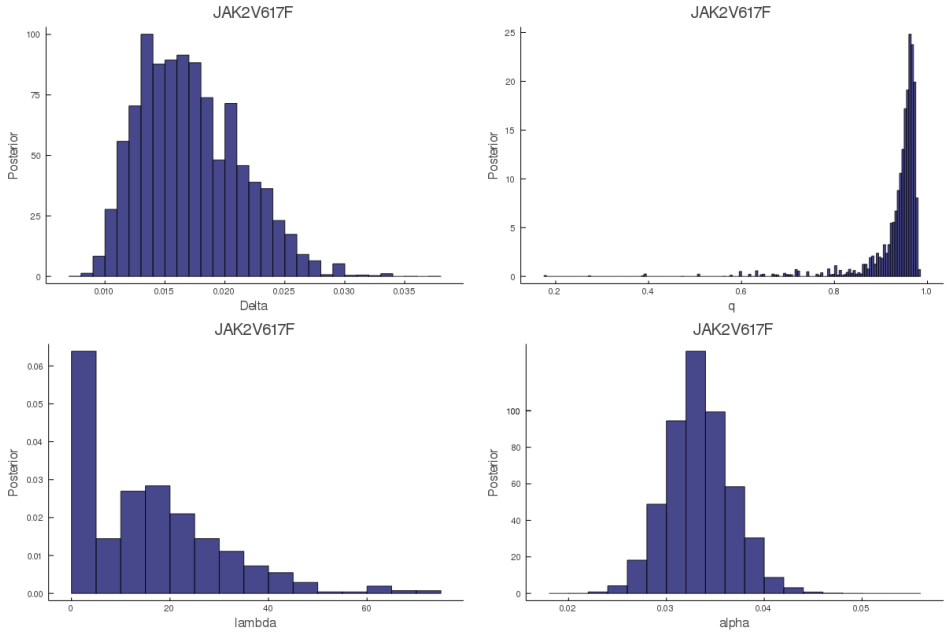

Figure D.2: Posterior distributions of $\Delta = p_2 - p_0$ (top left), the extinction probability $q = p_0/p_2$ (top right), α (bottom right) and λ (bottom left) for $JAK2^{V617F}$ patients.

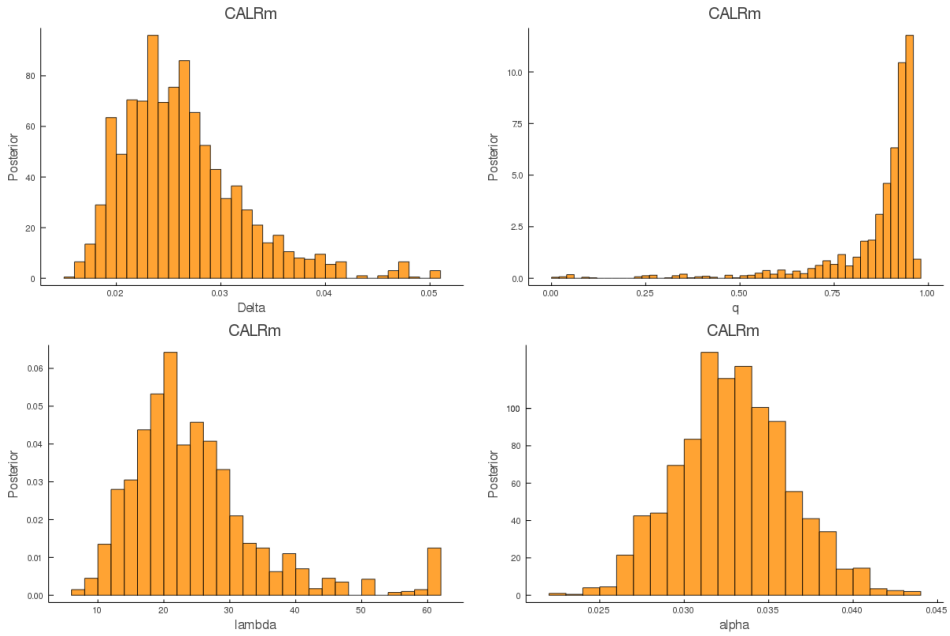

Figure D.3: Posterior distributions of $\Delta = p_2 - p_0$ (top left), the extinction probability $q = p_0/p_2$ (top right), α (bottom right) and λ (bottom left) for $CALR^m$ patients.

D.3 Leave-one-out analysis

To further assess the quality of the model fits, we proceed to a leave-one-out analysis. For each patient population (either $JAK2^{V617F}$ or $CALR^m$) of size N_p, we conduct N_p model calibrations $i \in \{1, \cdots, N_p\}$ in which individual i is removed. We then evaluate the capacity of the model (calibrated from the $N_p - 1$ observations) to generalize its results to an unseen individual. In particular, we focus on the ability to predict the time at which the clonal fraction of a given individual could be reached. It is the relevant information that we need to estimate accurately for our early screening methodology to be valid.

More precisely, for a given patient population, the whole dataset is denoted by $\mathcal{D}$. For a given individual i, with observations $(\hat{t}_i, \hat{\eta}_i)$, the dataset without them is denoted as $\mathcal{D}_{-i}$. The model is calibrated based on $\mathcal{D}_{-i}$. We estimate the posterior distribution of the parameter vector θ: $p[\theta|\mathcal{D}_{-i}]$.
In particular, we can analyze how $p[\Delta|\mathcal{D}_{-i}]$ deviates from $p[\Delta|\mathcal{D}]$ for each patient i, and according to whether or not they present other mutations (Fig. D.4).
This analysis does not reveal that including a patient with other mutations (than that of interest) would impact the estimations of the model parameters.

Then, for the given CF $\hat{\eta}_i$, we can estimate $p[t_i|\mathcal{D}_{-i}, \hat{\eta}_i]$, where t_i is the time at which $\hat{\eta}_i$ should be reached, that is, $\eta(t_i) = \hat{\eta}_i$. We numerically estimate the previous quantity $p[t_i|\mathcal{D}_{-i}, \hat{\eta}_i]$ by simulating 2,000 trajectories from our model with the parameter vector sampled from the posterior $p[\theta|\mathcal{D}_{-i}]$. We confront $p[t_i|\mathcal{D}_{-i}, \hat{\eta}_i]$ to the true observation time $\hat{t}_i$ (Fig. D.5).

To evaluate the accuracy of the prediction, we subdivide the period $[0, 100]$ years into twenty 5-years intervals:

$$I_1 = [0, 5], I_2 = [5, 10], \cdots, I_{19} = [90, 95], I_{20} = [95, 100]$$

We denote by $\hat{I}^i$ the 5-year interval that contains the observation time: $\hat{t}_i \in \hat{I}^i$. We compute:

$$\mathbb{P}[\hat{t}_i \in \hat{I}^i|\mathcal{D}_{-i}, \hat{\eta}_i] \tag{7}$$

We call the previous quantity "score" and compare it to the score that would have been obtained "by chance" (that is, with a uniform sampling), whose value is equal to $1/20 = 0.05$ (Fig. D.6).
The higher the score, the more accurate the prediction. For $JAK2^{V617F}$, only two over 11 individuals (18%) have a score lower than expected "by chance". For the others, and especially #2, #3, #4, #5 and #8, we predict quite accurately the period when their CF should be reached (with higher probabilities). We also get good results for $CALR^m$ patients, with, however, two of them (13%) having a lower score than expected "by chance", and three of them (20%) a score approximately equal to 0.05. Note that, because of the stochasticity of our model, we should not expect to have only excellent scores since the posterior distributions represented in Fig. D.5 are intended to represent variability over a population of patients.
The results of this study increases the confidence about the conclusions we drew from our early screening method.

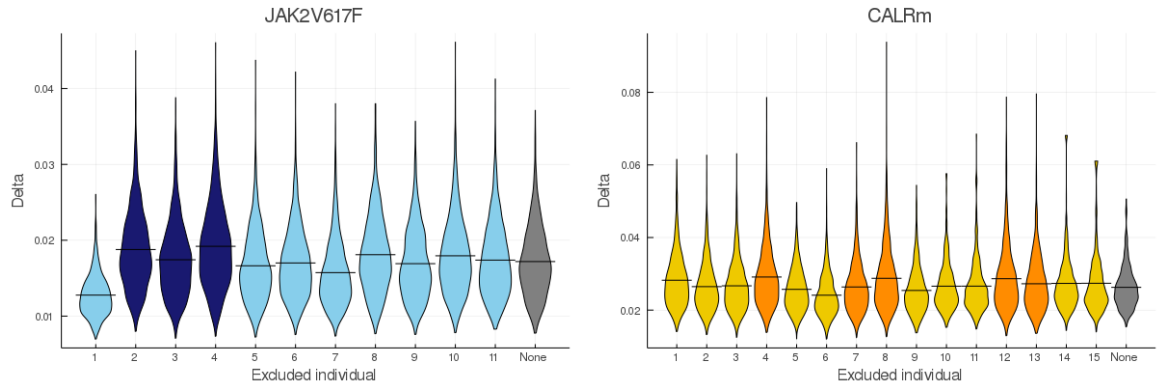

Figure D.4: Posterior distribution $p[\Delta|\mathcal{D}_{-i}]$ of parameter Δ when removing patient i (x-axis) of the $JAK2^{V617F}$ (left) or $CALR^{m}$ (right) patient populations. The right (gray) distribution represents the posterior distribution computed without excluding any individual. The horizontal black lines indicate mean posterior values. Individual with additional mutations are represented in dark.

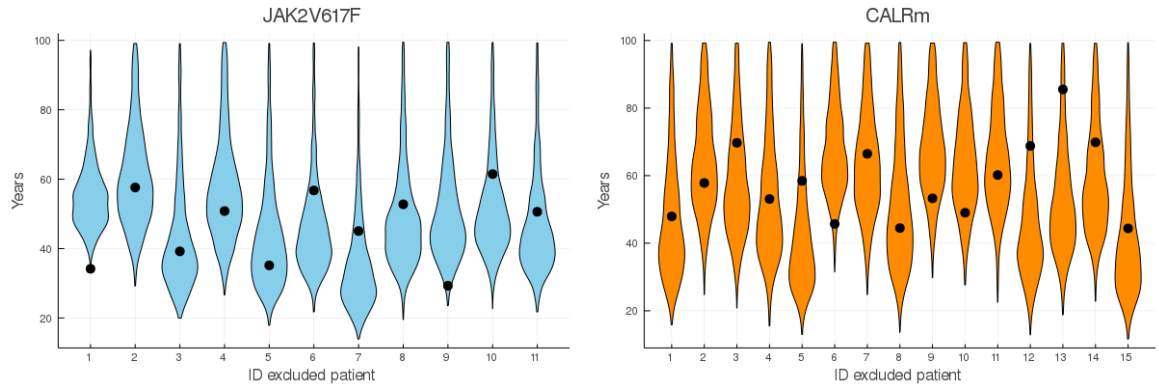

Figure D.5: Posterior distributions of the time t_i (y-axis) at which the observed CF $\hat{\eta}_i$ of patient i (x-axis) might be reached: $p[t_i|\mathcal{D}_{-i}, \hat{\eta}_i]$ for $JAK2^{V617F}$ (left) or $CALR^{m}$ (right) patient populations. Black points indicate $p[t_i = \hat{t}_i|\mathcal{D}_{-i}, \hat{\eta}_i]$

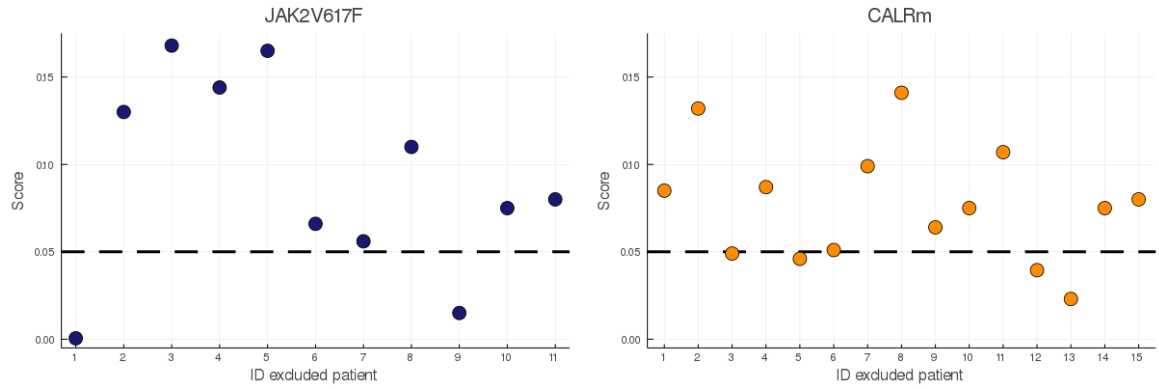

Figure D.6: Score - given by eq. (7) - for $JAK2^{V617F}$ (left) or $CALR^{m}$ (right) patients. We compare them to the score that might be expected by chance (equal to 0.05). High scores indicate that the time $\hat{t}_i$ at which the CF $\hat{\eta}_i$ of patient i is measured is near what would be expected with highest probability by the model (calibrated without patient i).

E Comparison with other studies for the $JAK2^{V617F}$ mutation

To further assess the validity of our model, we verify that our estimations in the case of the $JAK2^{V617F}$ mutation are consistent with those reported by others [11, 14, 12]. First, we focus on our estimates for the mean acquisition time λ, then for the proliferative advantage Δ.

E.1 Acquisition time

Van Egeren et al. [11] and Williams et al. [14] inferred, from the construction of phylogenetic trees, the individual acquisition time of the mutation $JAK2^{V617F}$ for several patients while we infer a mean acquisition time at the population level. We will confront our results with theirs. More precisely, Van Egeren et al. and Williams et al. estimate a period in which the mutation should have occurred.

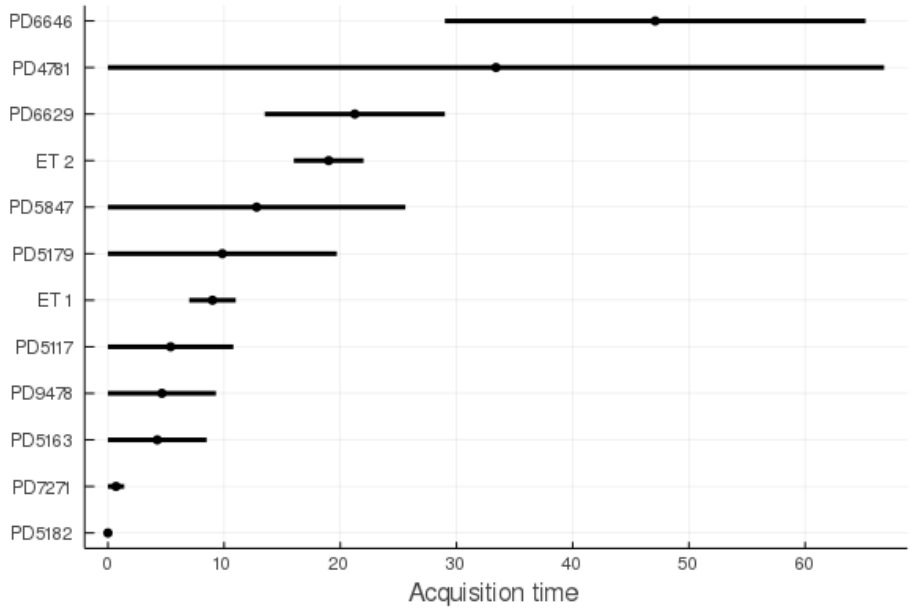

Figure E.1: Data from Williams et al. [14] (individuals whose ID begin with "PD") and from Van Egeren et al. [11] (Patients ET 1 and ET 2). We indicate the lower and upper estimates for the acquisition time, as reported in the corresponding articles. Black points indicate mean estimates (the mean value computed over the 12 individuals is equal to 14 years). Age values during fetal life (between 0 and 36 weeks post-conception) are set to $T_0 = 0$.

We report below their findings (Fig. E.1):

- PD7271: between 6.9 weeks (post conception) and 1.4 years
- PD5163: between 3.1 weeks (post conception) and 8.5 years
- PD5117: between 2.9 weeks (post conception) and 10.8 years
- PD5182: between 6.4 weeks and 32.8 weeks (post conception)
- PD5179: between 0 and 19.7 years
- PD6629: between 13.5 and 29 years
- PD5847: between 0 and 25.6 years
- PD9478: between 0 and 9.3 years

- PD6646: between 29 and 65.2 years
- PD4781: between 0 and 66.8 years
- ET1: at age 9 ± 2
- ET2: at age 19 ± 3

We denote this validation dataset by $\mathcal{D}'$. For each individual i, we have a lower and upper bound for the true acquisition time $T_{0,i} \in [\hat{T}_{inf,i}, \hat{T}_{sup,i}]$. Note that Williams et al. also reported acquisition ages in weeks post-conception, that is, they estimated an age of acquisition during fetal life. In our study, the whole period of fetal live is modeled as $T_0 = 0$. This is also why we have to authorize that $\lambda = 0$ (equivalent to $T_0 = 0$) with a non-zero probability.

As a first step, if we consider that the acquisition time for each individual is $\hat{T}_{0,i} = 0.5 \cdot (\hat{T}_{sup,i} - \hat{T}_{inf,i})$, a rough estimation for the mean acquisition time $\hat{\lambda}$ based on their dataset $\mathcal{D}'$ would be

$$\hat{\lambda} = \frac{1}{12} \sum_{i=1}^{12} \hat{T}_{0,i} = 14 \text{ years}$$

comparable with our findings (a mean value for λ estimated to 15.2 years).

Then, we propose a second approach that accounts for the uncertainty of the original dataset (that is, the lower and upper bounds). Our method here is based on two assumptions. First, we assume that $T_{0,i}$ (for individual i) is a random variable that can be equal to 0 with probability b or otherwise (with probability $1 - b$) is distributed over $\mathbb{R}^+$ following an exponential law of rate l^{-1}. This assumption is made to be in line with our model (see § B.4). In that case, we have $\lambda = \mathbb{E}[T_{0,i}] = b \times l$.
Second, we assume that $T_{0,i} - T_{inf,i} | T_{0,i} \sim \mathcal{E}(\mu)$ and $T_{sup,i} - T_{0,i} | T_{0,i} \sim \mathcal{E}(\mu)$ (with μ the same in both distributions). That is, we consider that the upper and lower bounds should be found "near" the true value of the acquisition time.
Under these two assumptions, we get the expression of the likelihood:

$$p[\mathcal{D}'|l, b] = \prod_{i=1}^{12} p[(\hat{T}_{inf,i}, \hat{T}_{sup,i})|l, b]$$

with, for $i \in \{1, \cdots, 12\}$:

$$\begin{aligned}
p[(\hat{T}_{inf,i}, \hat{T}_{sup,i})|l,b] &= \int_{\mathbb{R}} p[(\hat{T}_{inf,i}, \hat{T}_{sup,i})|T_{0,i} = t] \cdot p[T_{0,i} = t|l,b] \; dt \\
&= \int_{\hat{T}_{inf,i}}^{\hat{T}_{sup,i}} p[\hat{T}_{inf,i}|T_{0,i} = t] \cdot p[\hat{T}_{sup,i}|T_{0,i} = t] \cdot p[T_{0,i} = t|l,b] \; dt \\
&= \int_{\hat{T}_{inf,i}}^{\hat{T}_{sup,i}} \frac{1}{\mu} \exp(-\frac{1}{\mu}(t - \hat{T}_{inf,i})) \frac{1}{\mu} \exp(-\frac{1}{\mu}(\hat{T}_{sup,i} - t)) \cdot p[T_{0,i} = t|l,b] \; dt \\
&= \int_{\hat{T}_{inf,i}}^{\hat{T}_{sup,i}} \frac{1}{\mu^2} \exp(-\frac{1}{\mu}(\hat{T}_{sup,i} - \hat{T}_{inf,i})) \cdot p[T_{0,i} = t|l,b] \; dt \\
&= \frac{1}{\mu^2} \exp(-\frac{1}{\mu}(\hat{T}_{sup,i} - \hat{T}_{inf,i})) \int_{\hat{T}_{inf,i}}^{\hat{T}_{sup,i}} p[T_{0,i} = t|l,b] \; dt \\
&\propto \int_{\hat{T}_{inf,i}}^{\hat{T}_{sup,i}} p[T_{0,i} = t|l,b] \; dt \\
&= p[T_{0,i} \in [\hat{T}_{inf,i}, \hat{T}_{sup,i}]|l,b] \\
&= F_{l,b}(\hat{T}_{sup,i}) - F_{l,b}(\hat{T}_{inf,i})
\end{aligned}$$

with $F_{l,b}$ the cumulative density function of $T_{0,i}$.

We get the profiled log-likelihood of both parameters, displayed in Fig. E.2. Profiled log-likelihood for parameter b (and the same goes for l) is defined by:

$$\mathcal{L}_b = \max_l \log\left(p[\mathcal{D}'|l,b]\right)$$

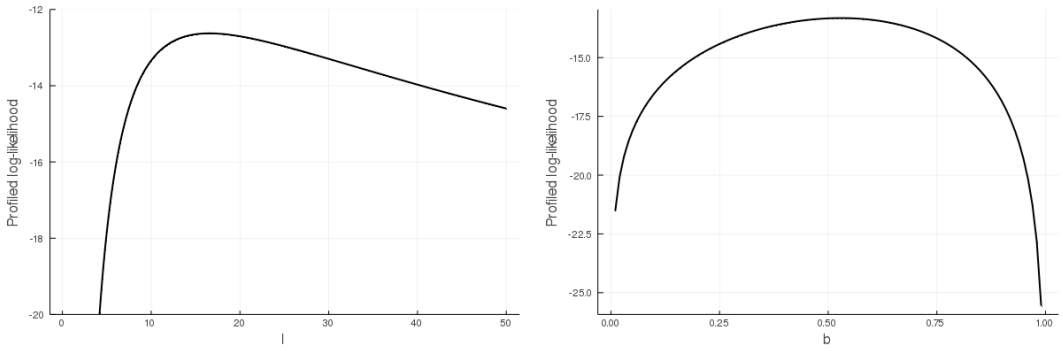

Figure E.2: Profiled log-likelihood of parameters l (left) and b (right). The maximum likelihood estimator (MLE) is $(\hat{l}, \hat{b}) = (17.71, 0.529)$.

We estimate the posterior distributions of the two parameters using a standard Metropolis-Hastings scheme (initialized at the MLE, 5 millions iterations, burn-out length of 2,000,000), with uniform prior distributions for b over $[0, 1]$ and l over [0,100]. Their posterior distributions are displayed in Fig. E.3.

Then, we can estimate the posterior distribution of the mean acquisition time, equal to $b \times l$ (see Fig. E.4). The mean acquisition time (mean posterior value) is estimated to 15.4 (median value equal

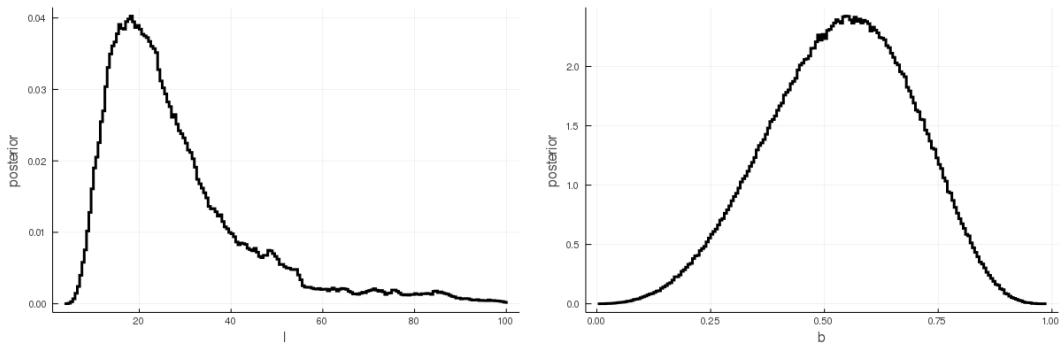

Figure E.3: Posterior distribution of parameters l (left) and b (right), given the validation dataset $\mathcal{D}'$.

to 12.5, and with 90% credibility interval: [4.0, 37.6]). Thus, with this second approach, we retrieve results that are consistent with ours.

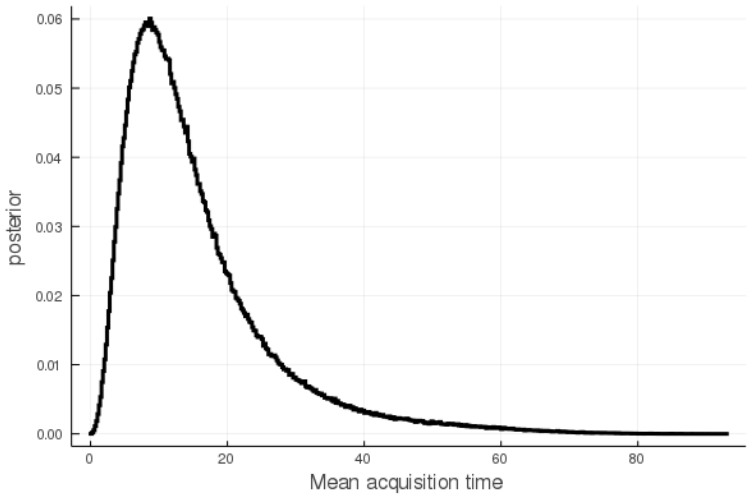

Figure E.4: Posterior distribution of the mean acquisition time (equal to $b \times l$) given the validation dataset $\mathcal{D}'$.

E.2 Fitness

Our model of the mutated HSC dynamics is not far from the one used by Watson et al. [12]. To describe the proliferative advantage of mutated clones, they introduce a fitness effect s. We can derive a relation between their parameter s and our parameter Δ. Indeed, according to Watson et al.:
"*In a time interval dt a single HSC can divide symmetrically producing two terminally differentiated cells [...] with probability D dt, divide symmetrically producing two stem cells with probability* $Bdt = (D + s)dt$*, [...]*" [12].
Thus, we derive the following relations $\alpha p_2 dt = (D + s)dt$ and $\alpha p_0 dt = D\ dt$, that is:

$$s = \alpha\Delta$$

Watson et al. estimated, for the fitness effect, $s = 14.6$ (% per year).
In our case, we estimate (mean posterior value) $\alpha\Delta = 20.4$ (% per year) with 95% credibility interval: [14.2 , 28.6]. Compared to their results, we estimate a higher fitness effect of the mutated $JAK2^{V617F}$ clone. This difference can be explained by the fact that Watson et al. studied clonal hematopoiesis, while we infer a proliferative advantage based on the observations from MPN patients.

References

[1] Beaumont, M. A., Cornuet, J.-M., Marin, J.-M., and Robert, C. P. Adaptive approximate bayesian computation. *Biometrika 96*, 4 (2009), 983–990.

[2] Darling, R., Norris, J. R., et al. Differential equation approximations for markov chains. *Probability surveys 5* (2008), 37–79.

[3] El-Khoury, M., Cabagnols, X., Mosca, M., Vertenoeil, G., Marzac, C., Favale, F., Bluteau, O., Lorre, F., Tisserand, A., Moraes, G. R., et al. Different impact of calreticulin mutations on human hematopoiesis in myeloproliferative neoplasms. *Oncogene 39*, 31 (2020), 5323–5337.

[4] Kimmel, M., and Axelrod, D. E. *Branching processes in biology*. Springer-Verlag, 2015.

[5] Kuhn, H. W. The hungarian method for the assignment problem. *Naval research logistics quarterly 2*, 1-2 (1955), 83–97.

[6] Lee-Six, H., Øbro, N. F., Shepherd, M. S., Grossmann, S., Dawson, K., Belmonte, M., Osborne, R. J., Huntly, B. J., Martincorena, I., Anderson, E., et al. Population dynamics of normal human blood inferred from somatic mutations. *Nature 561*, 7724 (2018), 473–478.

[7] Marin, J.-M., Pudlo, P., Robert, C. P., and Ryder, R. J. Approximate bayesian computational methods. *Statistics and Computing 22*, 6 (2012), 1167–1180.

[8] Mosca, M., Hermange, G., Tisserand, A., Noble, R., Marzac, C., Marty, C., Le Sueur, C., Campario, H., Vertenoeil, G., El-Khoury, M., et al. Inferring the dynamics of mutated hematopoietic stem and progenitor cells induced by ifnα in myeloproliferative neoplasms. *Blood* (2021).

[9] Munkres, J. Algorithms for the assignment and transportation problems. *Journal of the society for industrial and applied mathematics 5*, 1 (1957), 32–38.

[10] Sisson, S. A., Fan, Y., and Tanaka, M. M. Sequential monte carlo without likelihoods. *Proceedings of the National Academy of Sciences 104*, 6 (2007), 1760–1765.

[11] Van Egeren, D., Escabi, J., Nguyen, M., Liu, S., Reilly, C. R., Patel, S., Kamaz, B., Kalyva, M., DeAngelo, D. J., Galinsky, I., et al. Reconstructing the lineage histories and differentiation trajectories of individual cancer cells in myeloproliferative neoplasms. *Cell stem cell 28*, 3 (2021), 514–523.

[12] Watson, C. J., Papula, A., Poon, G. Y., Wong, W. H., Young, A. L., Druley, T. E., Fisher, D. S., and Blundell, J. R. The evolutionary dynamics and fitness landscape of clonal hematopoiesis. *Science 367*, 6485 (2020), 1449–1454.

[13] Wieland, F.-G., Hauber, A. L., Rosenblatt, M., Tönsing, C., and Timmer, J. On structural and practical identifiability. *Current Opinion in Systems Biology 25* (2021), 60–69.

[14] Williams, N., Lee, J., Mitchell, E., Moore, L., Baxter, E. J., Hewinson, J., Dawson, K. J., Menzies, A., Godfrey, A. L., Green, A. R., et al. Life histories of myeloproliferative neoplasms inferred from phylogenies. *Nature* (2022), 1–7.